ELSEVIER

Accuracy assessments of hyperspectral waveband performance for vegetation analysis applications

Prasad S. Thenkabail[a,*], Eden A. Enclona[b,c], Mark S. Ashton[b,c], Bauke Van Der Meer[d]

[a] International Water Management Institute (IWMI), PO Box 2075, Street 127, Sunil Mawatha, Pelawatte, Battaramulla, Colombo, Sri Lanka
[b] Center for Earth Observation (CEO), Yale University, PO Box 208109, New Haven, CT 06511, USA
[c] School of Forestry and Environmental Studies, Yale University, PO Box 208109, New Haven, CT 06511, USA
[d] International Institute of Tropical Agriculture (IITA), Oyo Road, Ibadan, Nigeria

Abstract

The main objectives of this research were to: (a) determine the best hyperspectral wavebands in the study of vegetation and agricultural crops over the spectral range of 400–2500 nm; and (b) assess the vegetation and agricultural crop classification accuracies achievable using the various combinations of the best hyperspectral narrow wavebands. The hyperspectral data were gathered for shrubs, grasses, weeds, and agricultural crop species from the four ecoregions of African savannas using a 1-nm-wide hand-held spectroradiometer but was aggregated to 10-nm-wide bandwidths to match the first spaceborne hyperspectral sensor, Hyperion. After accounting for atmospheric widows and/or areas of significant noise, a total of 168 narrowbands in 400–2500 nm was used in the analysis.

Rigorous data mining techniques consisting of principal component analysis (PCA), lambda–lambda R^2 models (LL R^2M), stepwise discriminant analysis (SDA), and derivative greenness vegetation indices (DGVI) established 22 optimal bands (in 400–2500 nm spectral range) that best characterize and classify vegetation and agricultural crops. Overall accuracies of over 90% were attained when the 13–22 best narrowbands were used in classifying vegetation and agricultural crop species. Beyond 22 bands, accuracies only increase marginally up to 30 bands. Accuracies become asymptotic or near zero beyond 30 bands, rendering 138 of the 168 narrowbands redundant in extracting vegetation and agricultural crop information. Relative to Landsat Enhanced Thematic Mapper plus (ETM+) broadbands, the best hyperspectral narrowbands provided an increased accuracy of 9–43% when classifying shrubs, weeds, grasses, and agricultural crop species.
© 2004 Elsevier Inc. All rights reserved.

Keywords: Hyperspectral wavebands; Optimal bands; Accuracy assessments; Vegetation analysis; African savannas; Spectroradiometer; Hyperion

1. Introduction

Hyperspectral remote sensor data can provide a significant enhancement of spectral measurement capabilities over conventional remote sensor systems that can be useful for the identification and subsequent modeling of terrestrial ecosystem characteristics (Kumar et al., 2001). For some applications, narrowbands located in specific portions of the spectrum are known to dramatically improve discrimination capabilities and classification accuracies for various vegetation and agricultural crops, relative to broadbands such as Landsat Thematic Mapper (TM) and Systeme Pour l'Observation de la Terre (SPOT) High-Resolution Visible (HRV) (Bork et al., 1999; Elvidge & Chen, 1995; Thenkabail, 2003).

Previous studies have determined that fine spectral resolution can be more important than high spatial resolution for mapping mangrove forests (Gao, 1999) and characterizing forest structure (Thenkabail et al., 2003). Gao (1999) found that mangrove forests were mapped with significantly greater accuracy using TM data (87.5–95%) than SPOT HRV data (67.5–77.5%). Thenkabail and Nolte (2003) determined that differences in rainforests resulting from moisture and topographic gradients were better detected using six-band Enhanced Thematic Mapper plus (ETM+) with 30-m spatial resolution vs. four-band IKONOS data with 4.0-m spatial resolution. The additional ETM+ bands in short-wave infrared (SWIR) explained approximately 20% additional variability in forest biotic characteristics when compared to IKONOS data without SWIR data.

* Corresponding author. Tel.: +94-1-867404, +94-1-869080, +94-1-869081, +94-1-872178, +94-1-872181; fax: +94-1-866854.

E-mail address: p.thenkabail@cgiar.org (P.S. Thenkabail).

Hyperspectral data can provide significant improvements in spectral information content when compared with broadbands for detecting plant stress (Carter, 1994, 1998); measuring chlorophyll content of plants (Blackburn, 1999); identifying small differences in percent green vegetation cover (McGwire et al., 2000); extracting biochemical variables such as nitrogen and lignin (Curran, 1994); discriminating land cover (LC) types (Janetos & Justice, 2000), crop moisture variations (Penuelas et al., 1993, 1995), and leaf pigment concentrations (Blackburn & Steele, 1999); modeling quantitative biophysical and yield characteristics of agricultural crops (Thenkabail, 2003); improving detection changes in sparse vegetation (Elvidge et al., 1993; Lyon et al., 1998); and assessing absolute water content in plant leaves (Bauer et al., 1981).
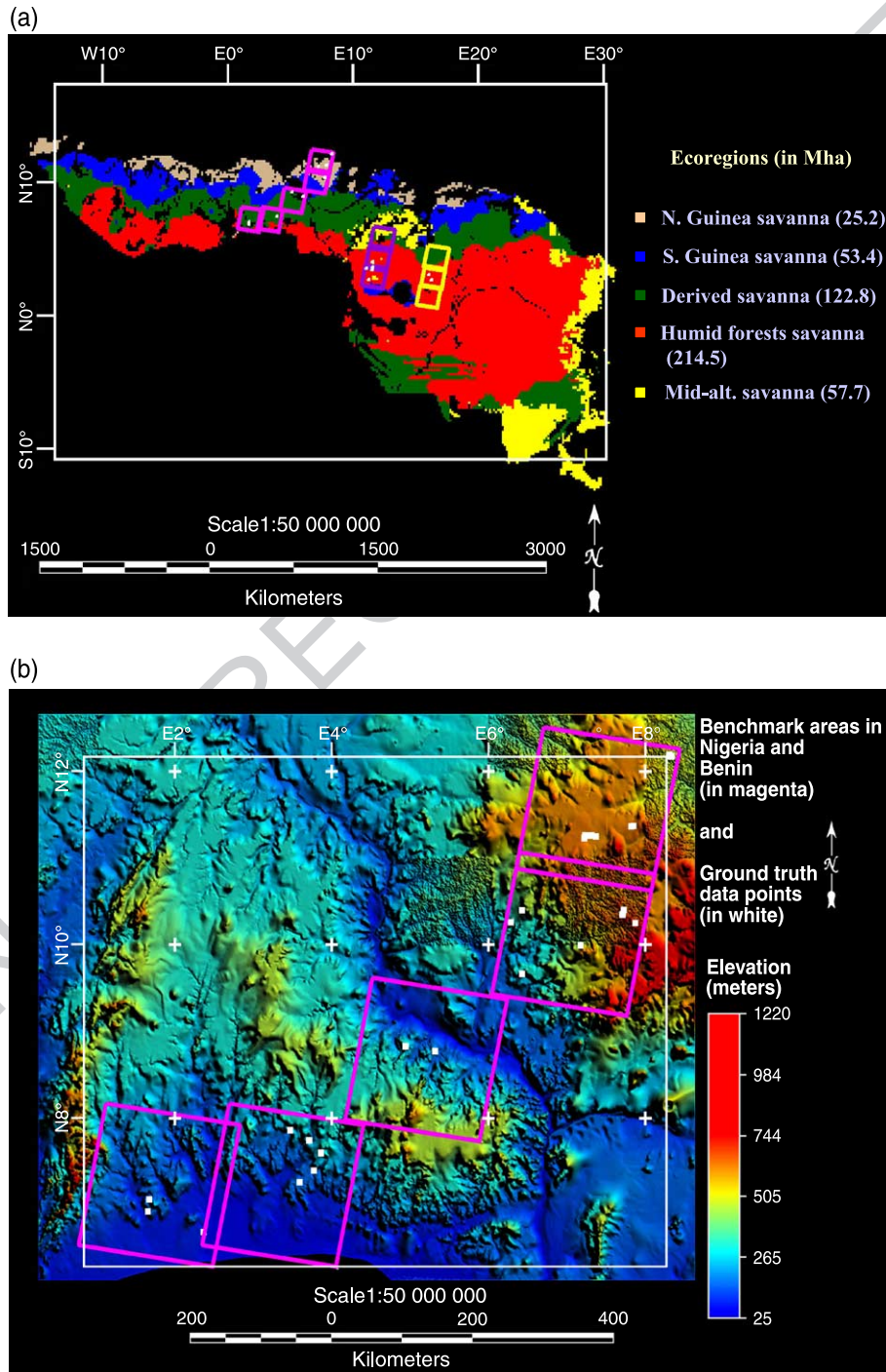

Fig. 1. (a) Ecoregions of West and Central African savannas and rainforests. (b) Hyperspectral data collection locations. Distribution of ground truth data points in the ecoregions of the West African savanna study area. [Note: At each white dot (groundtruth location), there are many ground truth points.]

However, it must be noted that using hyperspectral data is much more complex than multispectral data. Hyperspectral systems collect large volumes of data in a short time, leading to numerous complex technical issues. These issues include data storage volume, downlink or transmission bandwidth, real-time analog-to-digital bandwidth and resolution, atmospheric corrections, computing bottlenecks in data analysis, and new algorithms for data utilization. For example, data atmospheric correction is essential and extremely complex. Hyperion, the first spaceborne hyperspectral sensor onboard Earth Observing-1 (EO-1), gathers near-continuous 12-bit data in 220 discrete narrow spectral bands ranging from 0.4 to 2.5 μm at a spatial resolution of 30 m. A 1.0-km^2 Hyperion image contains approximately 0.5 megabytes (MB) compared to 0.007 MB in a six-band TM or ETM$^+$ data set. The volume of data collected using Hyperion for an area equivalent to Landsat TM image scene is about 15.5 gigabytes (GB), or equivalent to a space required to store 73 Landsat ETM$^+$ nonthermal bands. Such increase in data volume poses great challenge not only to data storage and archival but to data downlink (from satellite to the ground), data processing, and development of techniques and algorithms for data processing.

To best overcome these challenges, future generations of satellites are likely to carry specialized sensors—optimized to gather data for targeted applications (e.g., agriculture, environmental, etc.)—or to employ a narrow waveband hyperspectral sensor like Hyperion from which users with different application needs can extract appropriate optimal wavebands. In both cases, knowledge of (i) optimal narrowbands and (ii) potential improvements in accuracies over broadband sensors vs. cost will be required. Possibly, a comprehensive evaluation of hundreds of spectral wavebands and thousands of spectral indices may first be required to determine wavebands that provide the best information. An assessment of accuracies with increasing number of wavebands would be required to determine the impact of additional bands in discriminating, quantifying, classifying, and modeling vegetation and crop species and their characteristics.

Recent research has demonstrated that optimal information to quantify characteristics of forest canopies (Blackburn, 1998; Thenkabail et al., 2004), nonwoody vegetation (Broge & Leblanc, 2000), or agricultural crops (Carter, 1998; Thenkabail, 2002; Thenkabail et al., 2002), is present in a few specific narrowbands. However, each of the above studies was applied to only a limited number of vegetation species and used only a narrow portion of the spectrum (0.4–1.05 μm). There is a need to assess an optimal hyperspectral sensor configuration for a broader range of vegetation types over a greater spectral range (0.4–2.5 μm). Additionally, given the importance of SWIR bands in agriculture and vegetation studies (Thenkabail et al., 1994a, 1994b), it is important to determine the optimal SWIR spectral bands. The promise of SWIR bands has been recognized with the inclusion of these bands in series of new-generation sensors (Thenkabail, 2004) such as Moderate Resolution Spectroradiometer (MODIS; 1.628–2.155 μm), Advanced Spaceborne Thermal Emission and Reflection Radiometer (ASTER; 1.6–2.43 μm), ETM$^+$ (1.55–1.75 and 2.08–2.35 μm), Indian Remote Sensing Satellite (IRS-1D; 1.55–1.70 μm), and SPOT 4 (1.58–1.75 μm). However, most of these are broadbands that limit the fullest exploitation of the strengths of specific narrowbands.

The principle focus of this research was threefold: first, to determine optimal hyperspectral wavebands (0.4–2.5μm) that best characterize vegetation species and agricultural crops; second, to assess accuracies at which vegetation species can be classified and characterized using various narrow spectral bands; and, third, to compare the results of this study with independent studies using variable numbers of hyperspectral bands to classify agricultural crops (0.40–1.05 μm) in a desert margin benchmark area (see Thenkabail, 2002; Thenkabail et al., 2002).

1.1. Objectives

The specific objectives of this study were to: (a) determine optimal hyperspectral bands required to classify and characterize shrubs, grasses, weeds, and agricultural crop species; (b) study the role of SWIR bands relative to other wavelength portions in study of specific vegetation species; (c) build a spectral library of tropical shrubs, grasses, weeds, and crops; and (d) establish accuracies for classifying species types using independent data sources (i.e., Thenkabail et al., 2000, 2002) and compare their performance with the present study. Our working hypotheses was that significant increases in accuracies would be achieved with the addition of a few narrow SWIR bands to narrow VNIR (0.4–1.1 μm) bands.

1.2. Study area

The study was conducted in the representative benchmark areas in different ecoregions of West Africa (Fig. 1a). The characteristics of the ecoregions see shown in Table 1. For example, the Sudan savanna has a length of growing

Table 1

Ecoregions of WCA from which hyperspectral data on vegetation species and agricultural crops were collected for this study[a,b]

Ecoregion name	LGP[a]	Total area in WCA (Mha)
Sudan savanna	<151	N/A[c]
Northern Guinea savanna	151–180	25.2
Southern Guinea savanna	181–210	53.4
Derived savanna	211–270	122.8
Humid forests[d]	>270	214.5
Midaltitude savanna[d]	N/A[c]	57.7

[a] Ecoregions were based on the FAO (1978) LGP concept.
[b] Spatial distribution of ecoregions across WCA is shown in Fig. 1.
[c] Not available.
[d] Not part of this study.

period (LGP) of less than 151 days. These ecoregions cut across West and Central Africa (WCA; Fig. 1a) and are spread across large areas in WCA (Table 1). Spectral measurements were made across the entire range of elevation and climatic gradients encompassed by five ETM$^+$ images (Fig. 1b).

2. Methods

2.1. Hyperspectral data

Hyperspectral data were obtained from the 1-nm-wide narrowband FieldSpec Pro FR spectroradiometer manufactured by Analytical Spectral Devices (ASD) measuring spectra over a spectral range of 0.4–2.5 μm. Gathering spectra at any given location involved optimizing the integration time (typically set at 17 ms), providing foreoptic information, recording dark current, collecting white reference reflectance, and then obtaining target reflectance. An 18° field of view (FOV) was used. At each sampling location, target reflectance was measured from shrubs, grasses, weeds, and agricultural crop species. At each site, 10 reflectance measurements were consistently taken, along a transact, with a nadir view from a height of 3 m using a ladder. Spectroradiometer data of crops were analyzed using softwares PORTSPEC™ and VNIR™ supplied by the manufacturer of the instrument (Analytical Spectral Devices™), and Statistical Analysis System (SAS) version 6.12 (SAS Institute, 2002). The target reflectance is the ratio of energy reflected off the target (e.g., crops) to energy incident on the target (measured using a BaSO$_4$ white reference). Since the dark current varies with time and temperature, it was gathered for each integration time (virtually for each new reading):

$$\text{Reflectance} = \frac{(\text{target} - \text{dark current})}{(\text{reference} - \text{dark current})} \times 100\%$$

Since the dark current varies with time and temperature, it was gathered for each integration time (virtually for each new set of readings along a transect in a sample site location). Typically, 10–15 spectral measurements were made along a 30-m transect at each ground truth location. At each sample site, all the spectra along the 30-m transect were averaged to constitute a single representative spectrum. For further details on procedures for spectral data gathering, please refer to Thenkabail et al. (2000, 2002).

Over a thousand hyperspectral data field sample measurements were gathered for three shrubs, four grasses, five weeds, and six agricultural crop species (Figs. 2 and 3). Analysis was performed using the visible, near-infrared (NIR), and SWIR portions of the spectrum (0.35–2.50 μm) subdivided into 1.0-nm bandwidths. Hyperspectral data were then aggregated into 168 narrowbands, each 10.0 nm to match the characteristics of Hyperion wavebands over the

same spectral range. Broadband data for ETM$^+$ were simulated from the hyperspectral data. Simulation was performed by averaging narrowband spectral reflectivity over the range of wavelength coinciding with ETM$^+$ bands.

Mean values were plotted corresponding to hyperspectral by ecoregions (Fig. 1a and b), fallow systems (Fig. 2a), vegetation types (Fig. 2b), dominant weeds (Fig. 2c), and agriculture and other LC classes (Fig. 2d). The data were also gathered for specific species involving crops (Fig. 3a), shrubs (Fig. 3b), grasses (Fig. 3c), and weeds (Fig. 3d). When analyzing the data, the mean spectral plot of each sample location was used. The data in the spectral range of 1.35–1.44, 1.79–1.99, and 2.36–2.50 μm were seriously affected by atmospheric absorption (Figs. 2 and 3). Hence, the data in these wavelength portions were deleted from all analysis. Also, data in 0.35–0.39 μm were not considered due to spectral inconsistencies.

The remaining data were in 0.39–1.35, 1.44–1.79, and 1.99–2.36 μm and constitute a total of 1.68-μm wavelengths of good noise free data. Since each band was 1.0 nm wide, a total of 1680 bands was available for analysis. However, previous studies have shown that neighboring wavebands can frequently provide similar information, hence becoming redundant (Broge & Leblanc, 2000; Thenkabail et al., 2000, 2002, 2004). Also, the first spaceborne hyperspectral sensor, Hyperion, onboard EO-1, has a spectral range of 0.4–2.5 μm, with 10.0-nm bands. Given these facts, we reduced the 1680 bands into 168 bands, each of 10-nm-wide bands; we begin at 0.39 μm at 10.0-nm bandpasses to 2.4 μm, excluding atmospheric window bands (Table 2).

2.2. Band selection

No single best approach was available to determine the optimal number of bands required that provide the best estimates of forest or vegetation characteristics. Past research has incorporated reflectance from individual narrowbands (Mariotti et al., 1996), various ratio indices (Aoki et al., 1981; Carter, 1994; Lichtenthaler et al., 1996; Lyon et al., 1998), derivatives of reflectance spectra (Curran et al., 1991; Elvidge & Chen, 1995), or combinations of these (Thenkabail et al., 2000, 2002), and linear mixture modeling approach (Mass, 2000; McGwire et al., 2000). The optimal wavebands that best describe vegetation characteristics were determined based on a comprehensive analysis using (i) principal component analysis (PCA), (ii) lambda–lambda R^2 models (LL R^{2}M), (iii) stepwise discriminant analysis (SDA), and (iv) derivative greenness vegetation indices (DGVI). Overall accuracy and a κ statistic were calculated for vegetation cover types. All statistical analyses were performed using Statistical Analysis System (SAS Institute, 2002).

PCA was performed using the PROC PRINCOMP algorithm in SAS. The lambda (λ_i) vs. lambda (λ_j) R^2 models (LL R^{2}M) were performed to provide a rigorous search
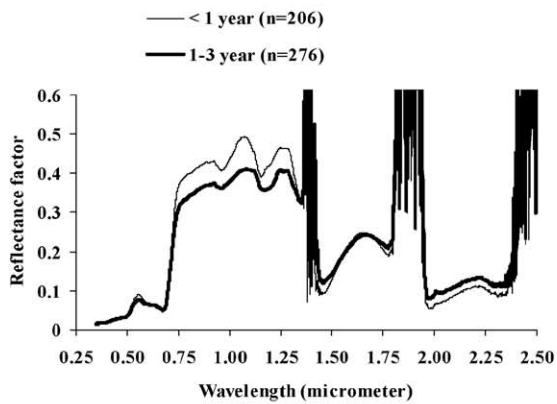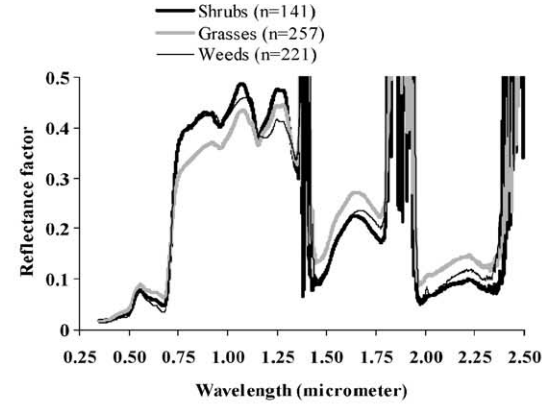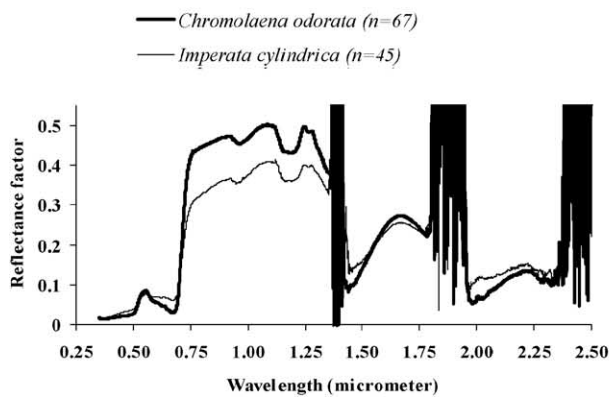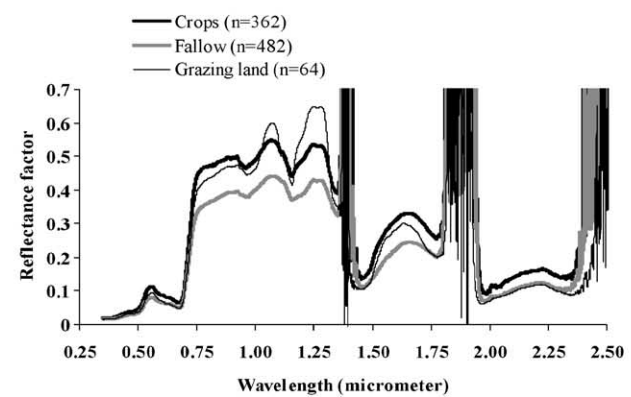
a. Fallow systems: <1 year and 1-3 years

b. Vegetation types: shrubs, grasses, and weeds

c. Dominant weeds: *Chromolaena odorata* and *Imperata cylindrica*

d. Agricultre and other land cover classes: crops, fallow areas, and grazing lands

Fig. 2. Hyperspectral datasets for land cover categories. Mean spectral profile of major land cover categories in African savannas: fallows, shrubs, grasses, weeds, and crops.

criterion or data-mining technique to highlight redundant wavebands from wavebands with unique information content (where i, j = 168 wavebands). A 168 (λ_i) × 168 (λ_j) band correlation (r) matrix was developed using PROC CORR algorithm of SAS. The correlation (r) values were converted to R^2 and reported. This provided 28,224 correlation coefficients (R^2) involving all possible combination of wavebands. We calculated R^2 values only below or above the diagonal of the 168 × 168 matrix, as values on either side of the diagonal were the transpose of one another. This resulted in R^2 values of 14,112. The lower the R^2 value, the less redundancy between two wavebands. Thus, lambda (λ_1)-vs.-lambda (λ_2) plotted areas with the least R^2 values for two wavebands were the areas with the highest information content (Figs. 4 and 5).

### 2.3. Data processing

SDA was used to discriminate or separate vegetation and crop species using Wilk's lambda, Pillai trace, and average squared canonical correlation (Thenkabail, 2002; Thenkabail et al., 2002). Stepwise selection was imitated with no variable in the model (SAS Institute, 2002). At each step, if

a band in the model failed to meet the criterion (f test), the worst variable was removed (SAS Institute, 2002). Otherwise, the band that contributed most to the discriminatory power of the model was entered. When all variables in the model met the criteria and the remaining variables were excluded, the stepwise selection process was stopped (SAS Institute, 2002). The resulting output had a Wilk's lambda, Pillai trace, and average squared canonical correlation. Based on the results of Thenkabail (2002), only the Wilk's lambda was reported since Pillai trace and average squared canonical correlation provide complimentary information. The values of Wilk's lambda were indicative of separability or discriminatory power of spectral bands (i.e., the less value of Wilk's lambda, the greater spectral differentiation between the species types).

A first-order DGVI was computed by taking near-continuous spectra along regions where there is significant or rapid change in slope of spectra per unit change in wavelength. Based on the observation of the spectra (Figs. 2 and 3) and literature (Elvidge & Chen, 1995; Thenkabail et al., 2000), these regions were located in 0.515–0.535 μm (DGVI1), 0.540–0.560 μm (DGVI2), 0.560–0.580 μm (DGVI3), 0.650–0.670 μm (DGVI4), 0.700–0.740 μm
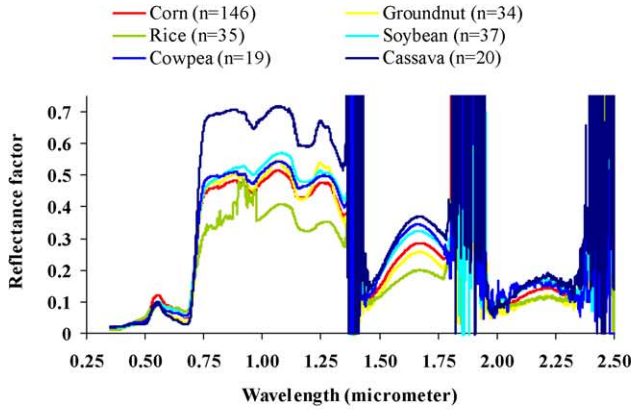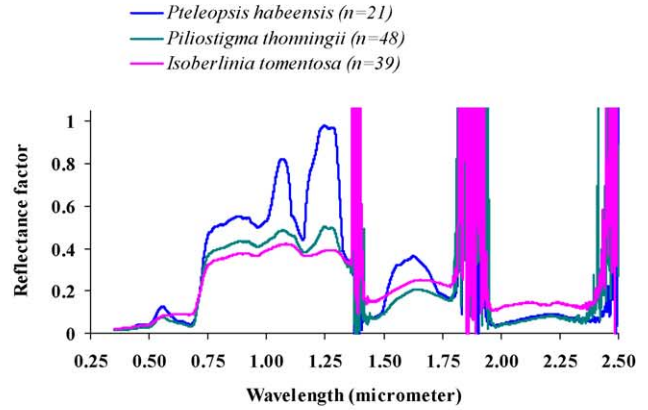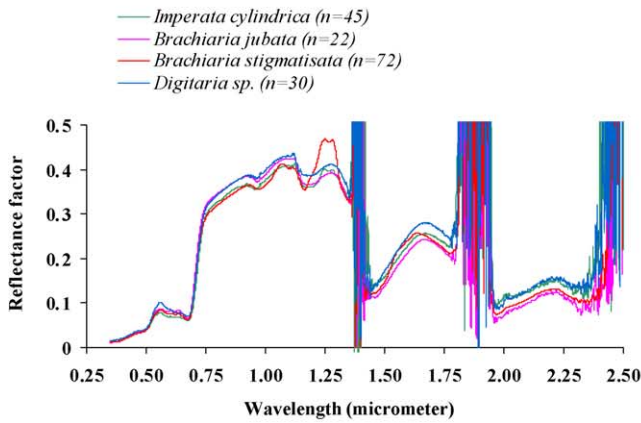
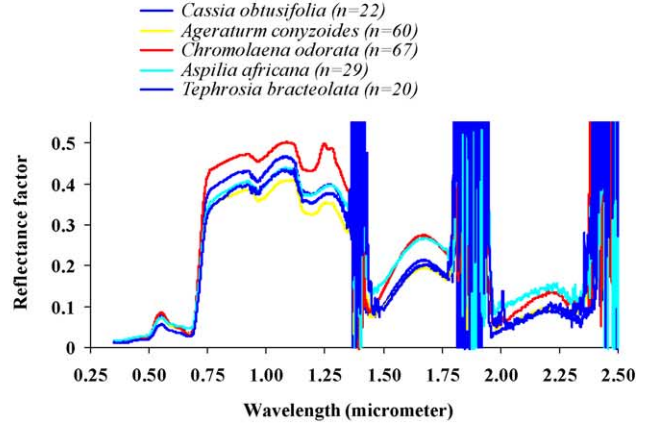Fig. 3. Hyperspectral datasets for vegetation and crop species. Mean spectral profile of major vegetation and crop species in the African savannas.

(DGVI5), 0.626–0.795 μm (DGVI6), 1.500–1.650 μm (DGVI7), and 2.080–2.350 μm (DGVI8). The chlorophyll red-edge portion is considered to have maximum sensitivity to changes in green vegetation per unit change in wavelength in the electromagnetic spectrum. The first-order DGVI (Elvidge & Chen, 1995) was computed using the equation:

$$DGVI = \sum_{\lambda_1}^{\lambda_n} \frac{[\rho'(\lambda_i) - \rho'(\lambda_j)]}{\Delta\lambda_i}, \tag{8}$$

where λ_i and λ_j are the wavelengths at the midpoints of bands i and j, ρ' is the first derivative of the reflectance, λ_1 is the start of a DGVHI waveband, and λ_n is the end of a DGHVI waveband. Where i and j are band numbers, λ = center of wavelength, and ρ' = first derivative reflectance.

2.4. Accuracy assessment

Classification accuracy assessments were performed using the error matrices generated from the discriminant model through SAS algorithm PROC DISCRIM (Congalton, 1988, 1991; Congalton & Mead, 1983). The discriminant model, also known as a classification criterion, was determined by a measure of generalized squared distance (Rao, 1973). The classification criterion was based on either the individual within-group covariance matrices or the pooled covariance matrix; it also accounted for the prior probabilities of the groups. Each observation, from an independent dataset, was placed in the class from which it has the smallest generalized squared distance. DISCRM was also used to compute the posterior probability of an observation belonging to each class. The generalized squared distance (D) function for crop types is:

$$D_j^2(X) = (X - \bar{X}_j)' \, COV^{-1}(X - \bar{X}_j) \tag{2}$$

where X is the vector of observations for a given pixel, $\bar{X}_j$ is the mean of all observations for crop type j, and COV is the covariance matrix:

$$\bar{P}_j r(j \mid X) = \exp\left(-.5\overset{2}{D(X)}_k\right) / SUMexp\left(-.5\overset{2}{D(X)}_k\right) \tag{3}$$

Error matrices were generated for different hyperspectral wavebands. This enabled us to see how the overall

t2.1	Table 2
t2.2	Hyperspectral data from this and two other independent studies

Band range (μm)	Hyperspectral data		Vegetation or crop species or LULC type (name)	Sample size (number)
	Total band width (μm)	Total number of bands (number)		
Hyperspectral data used in this study				
0.39–1.35	1.68 (in 0.39–2.36)	168 bands each,	Fallow systems	
1.44–1.79		10 nm (or 0.1 μm) wide	<1 year	206
1.99–2.36			1–3 years	276
			Vegetation types	
			Shrubs	141
			Grasses	257
			Weeds	221
			Dominant weeds	
			Chromolaena odorata	67
			Imperata cylindrica	45
			Agriculture and other LULC classes	
			Crops	362
			Fallow	482
			Grazing land	64
			Agricultural crops	
			Corn	146
			Groundnut	34
			Rice	64
			Soybean	37
			Cowpea	19
			Cassava	20
			Shrub species	
			Pteleopsis habeensis	21
			Piliostigma thonningii	48
			Isoberlinia tomentosa	39
			Grass species	
			Imperata cylindrica	45
			Brachiaria jubata	22
			Brachiaria stigmatisata	72
			Digitasia sp.	30
			Weed species	
			Cassia obtusifolia	22
			Ageraturm conyzoides	60
			Chromolaena odorata	67
			Aspilia africana	29
			Tephrosia bracteolata	20
Hyperspectral data from two other independent studies				
Thenkabail et al. (2000)				
0.395–1.01	0.615 (in 0.395–1.01)	430 bands each,	Agricultural crops	
		1.43 nm (or 0.0143 μm) wide	Cotton	73
			Potato	25
			Soybeans	27
			Corn	17
			Sunflower	9
Thenkabail et al. (2002)				
0.395–1.01	0.615 (in 0.395–1.01)	430 bands each,	Agricultural crops	
		1.43 nm (or 0.0143 μm) wide	Barley	44
			Wheat	64
			Lentil	23
			Cumin	17
			Chickpea	14
			Vetch	14

t2.60 Characteristics of the hyperspectral data gathered for this study were compared to hyperspectral data used in two other independent studies.

accuracies and Khat (see Thenkabail et al., 2002; Thenkabail et al., 2004) values increase with increases in input wavebands.

Overall accuracies were computed based on correctly classified pixels along the diagonal of an error matrix. Errors of commission and errors of omission were com-

Contour plot of R-squared values for all six crops and corn (*Zeamays*) using narrowband data
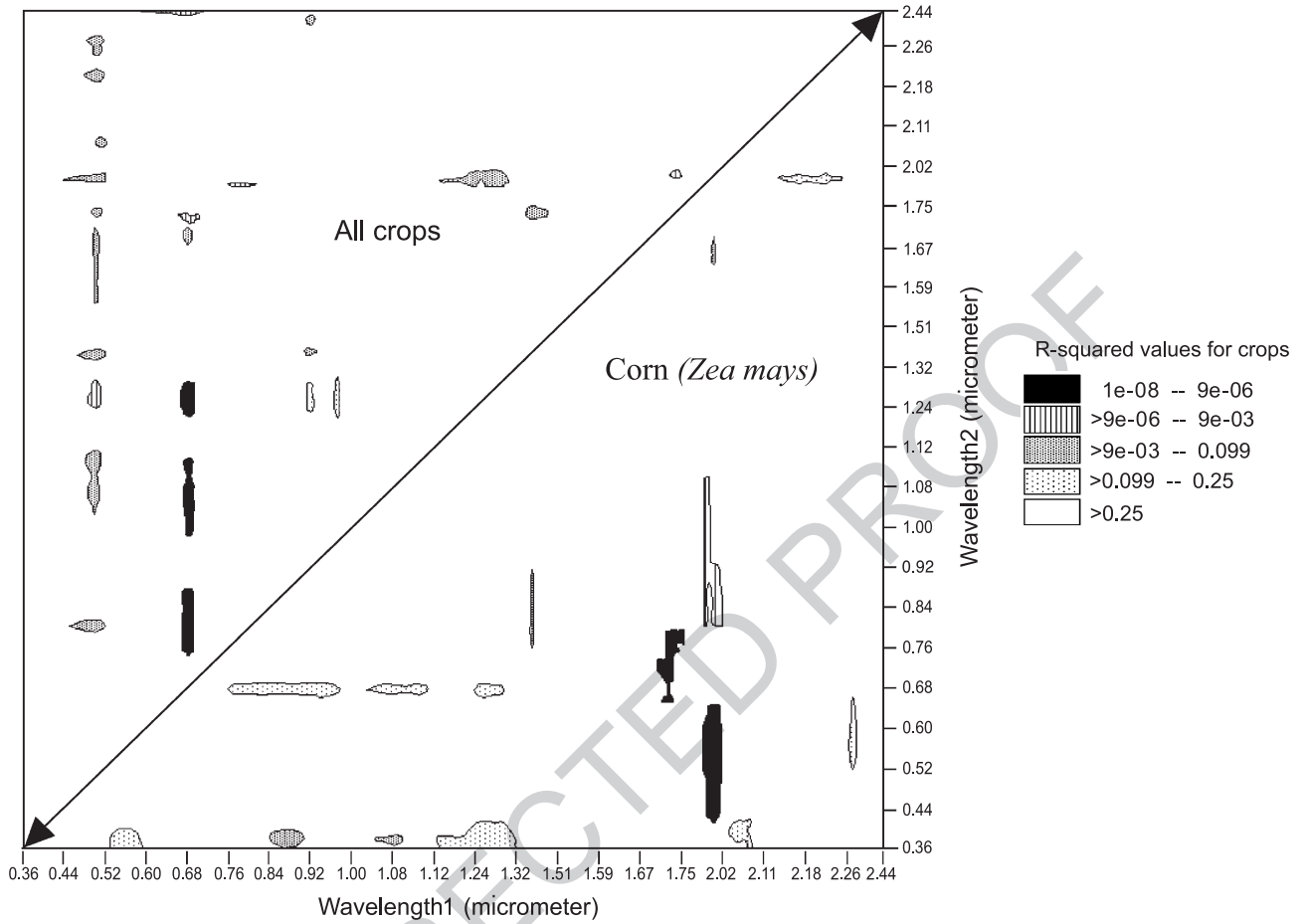

Fig. 4. Lambda–lambda R^2 plot. Areas of lowest R^2 values ("bull's eye") are the waveband regions with the least redundancy and the highest information content. Plot for all crop species (above the diagonal) and corn crop species (below the diagonal).

puted. The Khat was then computed so as to normalize the accuracy assessments between datasets and data types as follows:

$$K_{\text{hat}} = \left(N \sum_{i=1}^{r} X_{ii} - \sum_{i=1}^{r} X_{+i}X_{i+} \right) \Big/ \left(N^2 - \sum_{i=1}^{r} X_{i+}X_{+i} \right) \tag{4}$$

where r is the number of rows in the matrix; X_{ii} is the number of observations in row i and column i; X_{i+} and X_{+i} are the marginal totals of i and column i, respectively; and N is the total number of observations (Bishop et al., 1975).

3. Results and discussions

3.1. Principal component analysis

The first five principal components (PCs) explained 93–95% of the variability in the various weed species and agricultural crop species (Table 3). Thus, the next five PCs

only added a very small fraction of additional variability. Thereby, in order to explain $\geq 90\%$ of the variability, the 168 wavebands can be reduced to five PC wavebands (PC1–PC5), thus reducing data volume by approximately 97%. The new PC wavebands were computed using factor loadings (or eigen vectors) of each of the 168 wavebands and multiplying the factor loadings with their respective waveband reflectivity. The first five wavebands that provide the highest factor loadings are listed for PC1–PC5 (Table 3). The order in which the bands were listed indicates the magnitude or ranking for that band based on its factor loadings. For example, the PC1 for corn had wavebands centered at 1.675, 1.665, 1.645, 1.655, and 1.685 μm. This implied that the waveband centered at 1.675 μm had the highest factor loadings from all of the 168 wavebands in the entire spectral range of 0.35–2.50 μm. Thereby, the importance of the waveband was judged by its factor loadings. The early short-wave infrared (ESWIR) bands dominated the PC1 with a 62% frequency of occurrence, with the red bands in PC2 explaining 20% variability (Table 3). The far short-wave infrared (FSWIR) bands dominated PC3–PC5 in all, explaining an additional 12% of the variability. These

Contour plot of R-squared values for all five weeds and *Chromolaena odorata* using narrowband data
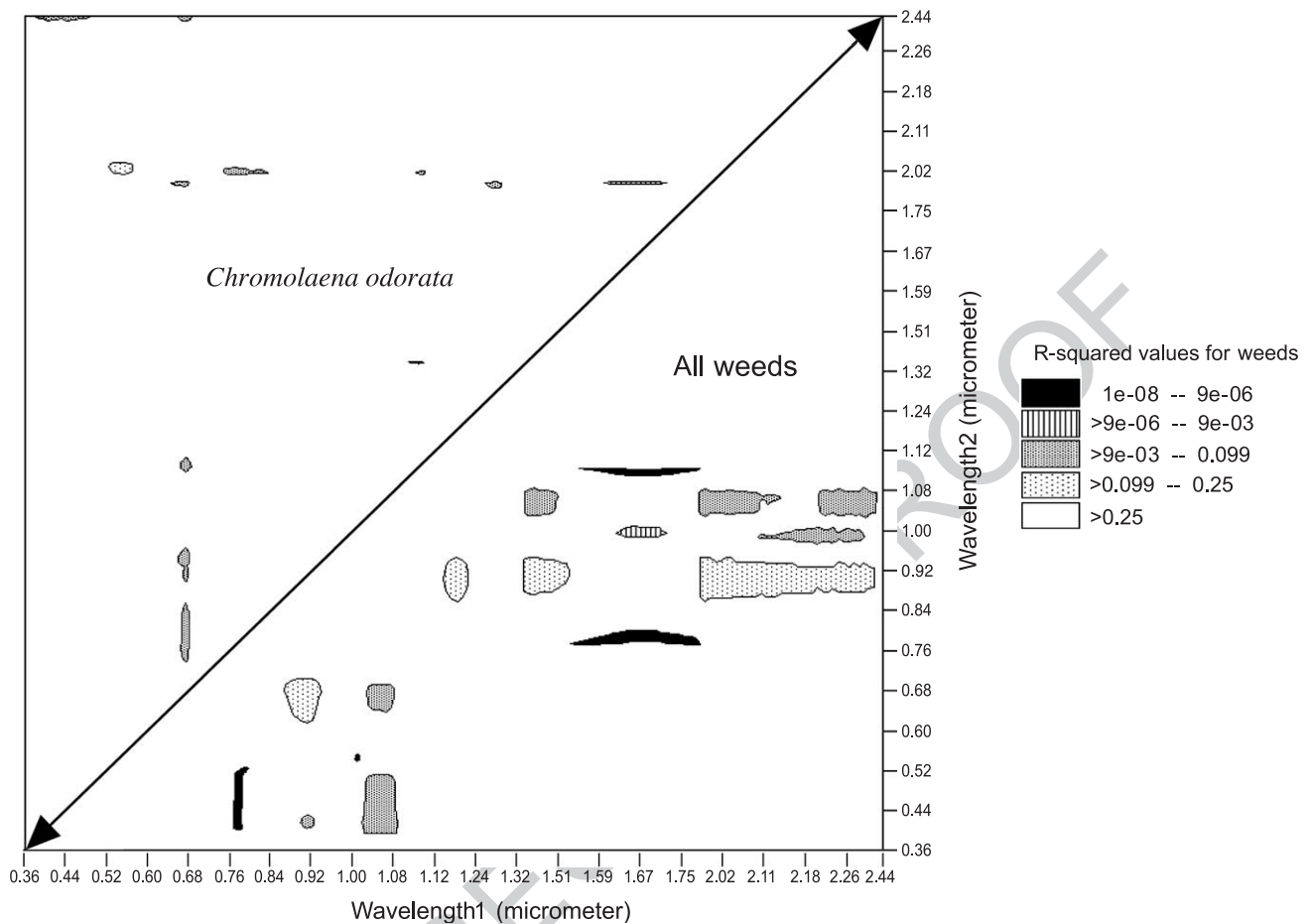

Fig. 5. Lambda–lambda R^2 plot. Areas of lowest R^2 values ("bull's eye") are the waveband regions with the least redundancy and the highest information content. Plot for all weed species (below the diagonal) and *Chromolaena odorata* weed species (above the diagonal).

results indicated the overall importance of red and SWIR wavebands.

3.2. Lambda–lambda R^2 models

For every vegetation and crop species, a rigorous search criterion was developed wherein every single waveband (λ_i) was correlated with every other waveband (λ_j), leading to lambda-vs.-lambda plots (Figs. 4 and 5). This helped to determine areas rich in information (areas of "bull's eye") and areas of data redundancy (areas of "empty spots") (Figs. 4 and 5). A very high correlation (R^2) between any two wavebands indicates similar or redundant information. The areas of lowest correlation between wavebands indicate that the two bands contained unique information about the species. To facilitate a rigorous search for waveband performance, we pooled the data for the major crop species and weed species for analysis (Figs. 4 and 5). Similar plots were established for all other crop species; however, they are not illustrated here (i.e., shrub, weed, and grass). The centers and widths of wavebands with the least redundancy were

summarized (Table 4). The most frequently occurring wavebands included the red, FSWIR, ESWIR, and late NIR. The waveband widths were optimized to provide maximum information and are determined from the lambda–lambda plots (Figs. 4 and 5). The optimal wavebands were mostly narrow (< 0.2 μm). The strength of the hyperspectral data is best tested by plotting lambda-vs.-lambda plots within a species category (e.g., different weed species) where spectral similarities are likely to be close. The cross-correlations between different species/LCs do not test the strength of hyperspectral data since these categories already have very distinct spectra (e.g., compare Fig. 3a–d).

3.3. Stepwise discriminant analysis: a comparison on hyperspectral and ETM+ data

The discriminatory power of hyperspectral data was assessed for the six agricultural crop species, three shrub species, four grass species, and five weed species (Fig. 6a). The lesser is the Wilk's lambda, the greater is the separability between species (Fig. 6a). Fig. 6a illustrates the

t3.1   Table 3

t3.2   PCA to select the optimal hyperspectral bands[a,b]

	Band centers (nm) with first 20 highest factor loadings					Percent variability explained						
	PCA1	PCA2	PCA3	PCA4	PCA5	PCA1	PCA2	PCA3	PCA4	PCA5	First five cumulative PCAs	First 10 cumulative PCAs
Ageratum conyzoides[c]	1.315;1.305; 1.295;1.195; 1.205	0.675;0.685; 0.665;2.102, 2.072	0.615;0.625; 0.635;0.605; 0.695	0.695;0.625; 0.635;2.022; 0.615	2.322;2.292; 2.282;2.332; 2.012	55	22	9	5	2	93	96
Dominating waveband[d]	FNIR	Red	Red	Red	FSWIR							
Cassia obtusifolia[c]	1.655;1.665; 1.675;1.705; 1.645	2.032;2.042; 2.072;2.082; 2.022	2.342;2.332; 2.272;2.062; 2.192	2.292;2.332; 2.262;2.322; 2.282	2.012;1.445; 2.342;0.405; 2.332	62	25	4	2	1	95	98
Dominating waveband[d]	ESWIR	FSWIR	FSWIR	FSWIR	FSWIR							
Chromolaena odorata[c]	1.705;1.695; 1.685;1.715; 1.675	0.675;0.665; 0.685;2.032; 0.655	2.342;2.002; 1.992;2.332; 2.012	0.705;0.575; 0.585;0.565; 0.535	1.245;1.255; 1.235;1.285; 1.275	77	9	3	2	1	93	96
Dominating waveband[d]	ESWIR	Red	FSWIR	Green	FNIR							
Cassava[e]	1.725;1.715; 1.705;1.575; 1.695	0.635;0.625; 0.695;0.615; 0.645	2.002;2.342; 2.322;2.282; 2.312	2.002;1.245; 1.255;1.235; 1.275	2.332;2.342; 2.322;1.982; 2.312	64	19	6	3	2	93	97
Dominating waveband[d]	ESWIR	Red	FSWIR	FNIR	FSWIR							
Corn[e]	1.675;1.665; 1.645;1.655; 1.685	2.032;2.052; 2.042;2.082; 2.072	2.002;2.012; 2.342;1.992; 2.022	0.405;0.415; 0.425;0.435; 1.445	2.342;2.002; 2.012;1.992; 1.982	67	16	8	2	2	95	97
Dominating waveband[d]	ESWIR	FSWIR	FSWIR	UV	FSWIR							
Rice[e]	1.155;1.315; 1.545;1.535; 1.555	0.915;0.905; 0.965;0.925; 0.435	1.992;2.002; 2.312;2.312; 1.982	2.342;2.322; 2.042;1.992; 2.282	2.262;2.272; 2.342;2.012; 2.312	53	25	8	3	2	92	96
Dominating waveband[d]	ESWIR	NIR peak	FSWIR	FSWIR	FSWIR							
Soybean[e]	1.645;1.245; 1.635;1.655; 1.625	1.715;2.292; 2.242;2.222; 2.202	2.322;2.332; 2.262;2.142; 2.172	1.755;2.092; 1.814;1.765; 1.745	2.072;1.765; 2.092;2.062; 1.755	56	27	10	2	1	96	99
Dominating waveband[d]	ESWIR	FSWIR	FSWIR	ESWIR	FSWIR							
Dominating waveband from all of the above[f]	ESWIR	Red	FSWIR	FSWIR	FSWIR							
Mean (%)						62	20	7	3	2	94	97

t3.21   PCA showing wavebands with highest factor loadings (eigen vectors) and the percent of variability explained by each principal component.

t3.22   [a] For each principal component, five wavebands that provide the highest factor loadings (eigen vectors) are listed.

[b] UV = ultraviolet (0.400–0.500 μm); FNIR = far near-infrared (1.051–1.300 μm); ESWIR = early short-wave infrared (1.301–1.900 μm); FSWIR = far

t3.23   short-wave infrared (1.901–2.500 μm).

t3.24   [c] Weed species.

t3.25   [d] Based on the five wavebands in each PCA with highest factor loadings (or highest eigen vectors).

t3.26   [e] Crop types.

t3.27   [f] Dominant waveband portion in all weed and crop species.

445 optimal Wilk's lambda values that were achieved using (i)
446 12 wavebands for differentiating the six agricultural crops
447 (0.00341); (ii) 9 wavebands for differentiating the three
448 shrub species (0.00207); (iii) 14 wavebands for differenti-
449 ating the four grass species (0.02545); and (iv) 12 wave-
450 bands for differentiating the five weed species (0.00291).
451 Beyond 14 bands, the decrease in Wilk's lambda was
452 marginal. Near-zero values of Wilk's lambda were achieved

453 between 11 and 20 narrowbands (Fig. 6a). Beyond 20
454 bands, the Wilk's lambda was asymptotic, except in the
455 case of fallows. For fallow species, a Wilk's lambda was
456 still relatively high with 0.33484, even when 26 wavebands
457 are used. The spectral data for fallows were composed of
458 over 25 species. Given this high diversity, a poor separabil-
459 ity for fallows using narrowbands was not surprising. The
460 most frequently occurring wavebands that achieved the

t4.1 Table 4
t4.2 LL R^2M to select optimal hyperspectral bands

Variable/ vegetation type	Wavebands with the least redundancy (rank)	R^2	Band centers and band widths of waveband 1 (nm)		Band centers and band widths of waveband 2 (nm)	
			W1	Diff. W1	W2	Diff. W2
(a) All crops	1	0.00000003	0.675	0.02	1.055	0.03
	2	0.00000207	0.675	0.02	1.245	0.05
	3	0.00000331	0.685	0.03	0.785	0.02
	4	0.00002000	1.725	0.03	2.002	0.03
	5	0.00007000	0.665	0.04	1.725	0.02
	6	0.00070000	0.775	0.03	1.992	0.02
	7	0.00368000	0.665	0.06	2.342	0.02
	8	0.00700000	0.495	0.02	1.255	0.05
	9	0.01242556	1.455	0.04	1.735	0.02
	10	0.01342817	0.495	0.02	1.125	0.06
	11	0.01684285	0.475	0.08	1.992	0.02
	12	0.01933768	0.505	0.03	1.445	0.01
	13	0.02022653	0.915	0.02	1.455	0.02
	14	0.02187145	1.225	0.05	1.992	0.03
	15	0.02348000	0.915	0.02	2.342	0.03
	16	0.02613719	0.495	0.03	1.735	0.04
	17	0.03300000	0.495	0.06	0.795	0.02
	18	0.04533918	0.495	0.03	2.202	0.02
	19	0.04634548	0.505	0.02	2.072	0
	20	0.04974684	0.495	0.15	2.272	0.03
	21	0.05842856	0.495	0.02	1.575	0.07
	22	0.06137511	0.675	0.02	1.695	0.03
	23	0.17418937	0.915	0.01	1.245	0.05
	24	0.18949480	0.965	0.01	1.245	0.08
(b) *Zea mays*	1	0.00000025	1.715	0.01	0.785	0.03
	2	0.00000207	1.982	0.01	0.555	0.11
	3	0.00002381	2.002	0.01	0.805	0.09
	4	0.02300379	1.455	0.04	0.875	0.14
	5	0.04616482	2.002	0.01	1.635	0.06
	6	0.05252347	0.885	0.06	0.375	0.04
	7	0.05714968	1.085	0.05	0.375	0.01
	8	0.10064122	0.935	0.15	0.675	0.01
	9	0.11136904	1.265	0.14	0.375	0.05
	10	0.12074930	1.115	0.11	0.675	0.01
	11	0.12117361	1.245	0.05	0.675	0.02
	12	0.14370165	2.172	0.04	2.002	0.01
	13	0.20969073	2.062	0.03	0.385	0.02
	14	0.21364733	2.272	0.01	0.575	0.13
	15	0.22229339	0.555	0.05	0.365	0.03
(c) All weeds	1	0.00000003	1.025	0.05	0.545	0.02
	2	0.0000003	1.585	0.08	1.115	0.01
	3	0.0000009	1.615	0.13	0.775	0.02
	4	0.000002	0.765	0.01	0.415	0.11
	5	0.0002	1.645	0.09	0.985	0.02
	6	0.014	2.242	0.23	0.985	0.02
	7	0.0202	1.025	0.06	0.395	0.04
	8	0.0402	2.242	0.11	1.075	0.03
	9	0.0417	1.495	0.05	1.035	0.04
	10	0.042	1.035	0.04	0.655	0.03
	11	0.05	2.092	0.11	1.035	0.04
	12	0.09	0.905	0.01	0.425	0.01
	13	0.101	1.525	0.21	0.925	0.03
	14	0.101	0.925	0.02	0.695	0.08
	15	0.105	2.212	0.35	0.885	0.04
	16	0.207	1.205	0.03	0.885	0.08
(d) *Chromolaena odorata*	1	0.02	0.675	0.02	2.342	0.01
	2	0.0428	1.275	0.03	2.002	0.01
	3	0.046	0.675	0.01	0.935	0.06
	4	0.05	0.665	0.08	2.002	0.01

Table 4 (*continued*)

Variable/ vegetation type	Wavebands with the least redundancy (rank)	R^2	Band centers and band widths of waveband 1 (nm)		Band centers and band widths of waveband 2 (nm)	
			W1	Diff. W1	W2	Diff. W2
(d) *Chromolaena odorata*	5	0.051	0.405	0.1	0.2342	0.01
	6	0.054	0.675	0.01	0.765	0.11
	7	0.061	1.135	0.03	1.445	0.01
	8	0.0701	0.765	0.09	2.022	0.014
	9	0.073	0.675	0.02	1.135	0.03
	10	0.083	1.135	0.04	2.022	0.02
	11	0.0861	1.645	0.12	2.002	0.01
	12	0.17	0.555	0.04	2.032	0.01

Lambda–lambda R^2 models (LL R^{2}M) to select waveband centers and widths for (a) all crops, (b) corn crop (*Zea mays*), (c) all weeds, and (d) *Chromolaena odorata* weeds.

optimal Wilk's lambda values for shrubs, grasses, weeds, row crops, and fallows were centered at 1.215, 0.73, 1.245, and 1.285 μm, respectively.

In comparison to narrowband performance, the simulated broadbands of ETM$^+$ perform poorly (Fig. 6a and b). The broadband Wilk's lambda values were significantly higher even when all six ETM$^+$ bands were used in separating three shrubs species (0.123931), four grass species (0.339395), five weed species (0.042331), and six crop species (0.10782) (Fig. 6b). These results indicated that the real strength of narrowband data was in separating vegetation and crop species when compared to broadband data. We will not repeat the comparison of ETM$^+$ and hyperspectral data using other methods, since the results were similar (see also Fig. 9a).

3.4. Derivative greenness vegetation index

The mean first-order DGVI values for various LC themes, species categories of vegetation and crops, were computed for specific wavelength portions (DGVI1–DGVI8) of the spectrum (Table 5). Nonparametric least significant (LS) tests on the means were established at ≥95% confidence interval. Significant differences in the mean values between any two categories were established for each of the eight DGVI induced at ≥95%. For example, in the 0.700–0.740 μm wavelength portion of the spectrum, the values for *Chromolaenea odorata* (Table 5) with a mean DGVI5 of 0.3005, and for *Imperata cylindrica* (Table 5) with a mean DGVI5 of 0.1737, were significantly different at ≥95% (Table 5). The DGVI8 for the same two species was not significantly different (Table 5). The mean DGVI5 values for weed species were significantly different between the species *Ageratum conyzoides* and *Aspilia africana*, but there was no significance with others. Of the eight DGVI types, the DGVI5 (0.700–0.740 μm) had the highest (16) cases where any two categories of vegetation or crops species were significantly different (Table 5). This was followed by DGVI6 (0.626–0.795 μm) with 14 cases, DGVI7 (1.500–1.650 μm) with 13 cases, and DGVI3 (0.560–0.580 μm), DGVI4 (0.650–0.670 μm), and DGVI8 (2.080–2.350 μm) with 10 cases each. The 0.700–0.740 μm range (DGVI5) represents the red-edge portion of the spectrum and indicates that this portion is the best portion for the computation of DGVIs. Elvidge and Chen (1995) had suggested computing DGVI6 that encompasses a larger spectral domain and has found the second best portion. But this portion includes a portion of the red and a portion of NIR. However, DGVI7 in the SWIR portion (1.500–1.650 μm) was able to differentiate three different combinations of shrub species, which the DGVI5 or DGVI6 failed to achieve. DGVI4 was better than other DGVIs in differentiating grass species.

3.5. Waveband optimization

The wavebands that provide the best results in the first three methods (PCA, LL R^{2}M, and SDA) were pooled together in order to determine their frequency of occurrence in the 0.395–2.500 μm range (Fig. 7). The two most frequently occurring wavebands, in the order of ranking, had waveband ranges of 0.675–0.695 and 1.985–2.015 μm (Table 6). Bands ranked second were in the waveband ranges 1.235–1.255 and 2.315–2.345 μm. The other rankings are listed in Table 6. Some other wavebands such as 1.675 μm were heavily involved in PCA1, which explains an overwhelming proportion (65%) of the total variability. PCA2 explained 19% variability. The average total variability explained by PCA3, PCA4, and PCA5 for weed and crop species was only 11%. Thereby, when a waveband occurs in PCA1, it gets sixfold weightage, compared to twofold for PCA2, and no weightage for PCA3 thereof. This approach normalizes the importance of wavebands.

The four methods (PCA, LL R^{2}M, SDA, and DGVI; Sections 3.1, 3.2, 3.3, and 3.4) provide complimentary and supplementary information. The PCA explains variability in data and reduces data redundancy; LL R^{2}M eliminates all redundant bands and provides wavebands that best model vegetation characteristics; and the SDA tests the strength of data in separating or discriminating species types. DGVI integrates the near-continuous data over a region of wavelength highlighting how spectral slopes are sensitive to changes in biophysical and biochemical properties of vegetation and crops. In the process, each one of the methods
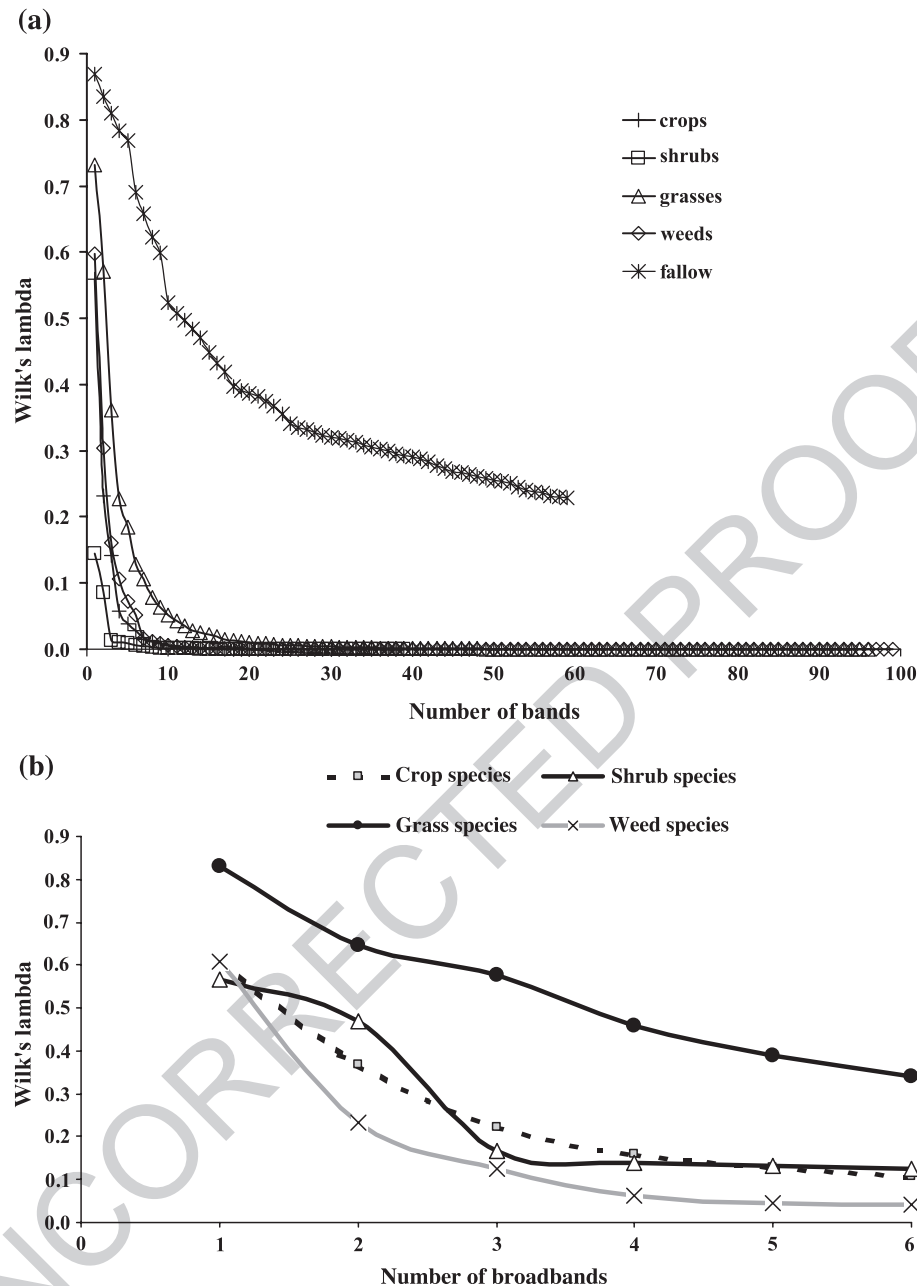
Fig. 6. (a) SDA to discriminate species using ETM⁺ narrowbands. Vegetation and crop species separability (or discrimination power) using narrowbands as determined using SDA (Wilk's lambda). The lesser is the Wilk's lambda, the greater is the discrimination power. (b) SDA to discriminate species using ETM⁺ broadbands. Vegetation and crop species separability (or discrimination power) using ETM⁺ broadbands as determined using SDA (Wilk's lambda). The lesser is the Wilk's lambda, the greater is the discrimination power.

543 highlights wavebands that are most sensitive. By pooling
544 the wavebands from these methods, we determine the
545 frequency of occurrence of wavebands leading to a recom-
546 mendation of 22 optimal wavebands (Fig. 7; Table 6).
547 The wavebands listed in Table 6 have a high level of
548 relevance in providing various vegetation or crop character-
549 istics as determined through findings from various research-
550 ers as discussed below. The waveband centered at 0.495 μm
551 (Table 6) is sensitive to carotenoid pigments (Blackburn,
552 1998; Tucker, 1977). Strong relationships with total chlo-

553 rophyll and nitrogen content were detected at 0.555 nm
554 (Blackburn, 1999; Schepers et al., 1996). Wavebands 0.655
555 and 0.675 nm vary significantly due to changes in factors
556 such as biomass, LAI, soil background, cultivars types,
557 canopy structure, nitrogen, moisture, and stress in plants
558 (Blackburn, 1998; Carter, 1998; Elvidge & Chen, 1995;
559 Thenkabail et al., 2000, 2002). The greatest crop–soil
560 contrast is around 0.675 μm for most crops in most growing
561 conditions (Thenkabail et al., 2000). Plant stress is best
562 detected at red-edge bands centered at 0.705 and 0.735 μm

t5.1 Table 5

t5.2 DGVIs and species discrimination

Category	ID	Subcategory		Waveband and wavelength (μm)							
			Sample size	DGVI1 0.515−0.535	DGVI2 0.540−0.560	DGVI3 0.560−0.580	DGVI4 0.650−0.670	DGVI5 0.700−0.740	DGVI6 0.626−0.795	DGVI7 1.500−1.650	DGVI8 2.080−2.350
Fallow areas											
	A	<1 year	221	0.0317	0.0083	− 0.0141	− 0.0086	0.2359	0.3351	0.1212	0.0165
	B	1−3 years	262	0.0238	0.0056	− 0.0092	− 0.0062	0.1903	0.2717	0.0991	0.0331
		Significance[a]		AB							
Land cover vegetation type											
	C	Shrubs	131	0.0262	0.0082	− 0.0104	− 0.0066	0.2285	0.3239	0.1052	0.0038
	D	Grasses	267	0.0263	0.0079	− 0.0091	− 0.0069	0.1794	0.2680	0.1137	0.0310
	E	Weeds	229	0.0314	0.0044	− 0.0164	− 0.0077	0.2545	0.3490	0.1123	0.0416
		Significance[a]			CE, DE	CE, DE		CD, DE			CD
Fallow land cover species											
	F	*Chromolaena odorata*	67	0.0356	0.0028	− 0.0200	− 0.0110	0.3005	0.3973	0.1324	0.0414
	G	*Imperata cylindrica*	45	0.0215	0.0058	− 0.0073	− 0.0043	0.1737	0.2577	0.0965	0.0391
		Significance[a]		FG		FG	FG	FG	FG	FG	
Major land use											
	H	Crops	327	0.0388	0.0064	− 0.0207	− 0.0100	0.3152	0.4268	0.1420	0.0119
	I	Fallow	480	0.0273	0.0067	− 0.0117	− 0.0073	0.2096	0.2900	0.1102	0.0223
	J	Grazing land	83	0.0384	0.0100	− 0.0216	− 0.0078	0.3274	0.4497	0.1600	0.0017
		Significance[a]		HI		HI	HI	HI, IJ	HI, IJ	HI	
Major species											
Agricultural crops											
	K	Cassava (*Manihot esculenta*)	20	0.046	0.002	− 0.031	− 0.007	0.503	0.650	0.175	0.073
	L	Corn (*Zea mays*)	146	0.047	0.007	− 0.024	− 0.014	0.289	0.386	0.137	0.011
	M	Cowpea (*Vigna unguiculata*)	19	0.032	0.006	− 0.016	− 0.004	0.332	0.433	0.156	0.045

t5											
t5.32	N	Groundnut (*Arachis hypogaea*)	34	0.035	0.004	−0.020	−0.009	0.322	0.426	0.128	0.008
t5.33	O	Rice (*Oryza sativa*)	35	0.008	0.012	−0.005	−0.007	0.150	0.263	0.083	0.066
t5.34	P	Soybean (*Glycine max*)	37	0.039	0.008	−0.015	−0.010	0.287	0.413	0.140	0.022
t5.35		Significance[a]		KO, MO, NO, OP	KO, NO	KO, KP, LO, NO	KL, LM, LN, LO	KL, KM, KN, KO, KP, LO, MO, NO, OP	KL, KM, KN, KO, KP, LO, MO, NO, OP	KL, KN, KO, LO, MO, NO, OP	KL, KM, KN, KP, LM, LO, MO, NO, OP
t5.36	Shrubs										
t5.37	Q	*Isoberlinia tomentosa*	39	0.020	0.011	0.002	−0.002	0.174	0.259	0.079	0.008
t5.38	R	*Piliostigma thonningii*	38	0.028	0.008	−0.015	−0.009	0.242	0.340	0.115	0.005
t5.39	S	*Pteleopsis habeensis*	20	0.049	0.017	−0.027	−0.008	0.324	0.449	0.214	0.000
t5.40		Significance[a]		QS		QR, QS	QR	QS	QS		QR, QS, RS
t5.41	Grasses										
t5.42	T	*Brachiaria jubata*	32	0.025	0.006	−0.008	−0.010	0.197	0.296	0.104	0.015
t5.43	U	*Brachiaria stigmatisata*	72	0.024	0.008	−0.007	−0.008	0.157	0.244	0.110	0.006
t5.44	V	*Digitaria* sp.	30	0.031	0.012	−0.009	−0.003	0.173	0.263	0.107	0.032
t5.45	W	*Imperata cylindrica*	45	0.022	0.006	−0.007	−0.004	0.174	0.258	0.096	0.039
t5.46		Significance[a]					TV, TW				
t5.47	Weeds										
t5.48	X	*Ageratum conyzoides*	60	0.028	0.003	−0.015	−0.008	0.222	0.311	0.094	0.041
t5.49	Y	*Aspilia africana*	29	0.025	0.004	−0.012	−0.003	0.223	0.318	0.104	0.037
t5.50	Z	*Cassia obtusifolia*	22	0.032	0.004	−0.017	−0.007	0.258	0.351	0.108	0.011
t5.51	Aa	*Chromolaena odorata*	67	0.036	0.003	−0.020	−0.011	0.301	0.397	0.132	0.041
t5.52	Ab	*Tephrosia bracteolata*	20	0.022	0.002	−0.012	−0.005	0.231	0.323	0.105	0.054
t5.53		Significance[a]					YAb	XY	XAa	XAa	
t5.54		Total cases of significant differences		8	4	10	10	16	14	13	10

t5.55 DGVIs for vegetation and crop separability or discrimination.

t5.56 [a] Significant differences at 95% confidence level or higher are reported. For example, for DGVI5 cassava (letter K, mean DGVI5 = 0.503) and corn (letter L, mean DGVI5 = 0.289) were significantly different (indicated by "KL") at 95% or higher confidence level.
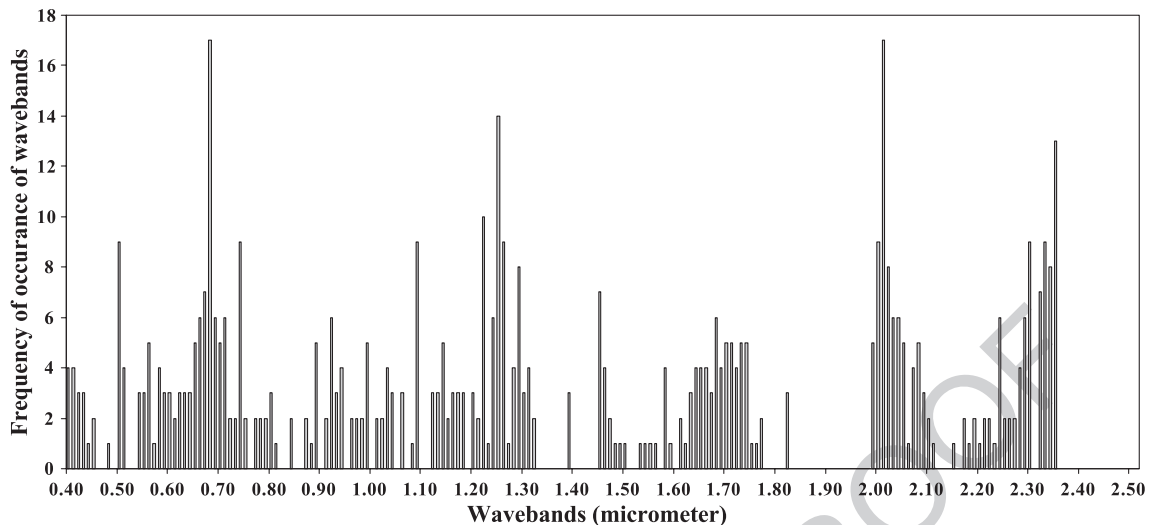
Fig. 7. Frequency of occurrence of the narrowbands in 0.400–2.500 μm. Frequency determined based on (a) PCA, (b) LL R^{2}M, and (c) SDA using Wilk's lambda.

(Elvidge & Chen, 1995). These bands also provide additional information about chlorophyll and nitrogen status of plants (Carter, 1994; Clevers, 1999; Elvidge & Chen, 1995; Shaw et al., 1998). Strong reflectance from healthy vegetation and correlation with total chlorophyll were detected at 0.886 μm (Schepers et al., 1996). Around 0.915 μm is the region of peak or maximum reflectance region of the NIR spectrum for certain types and/or growth stages of vegetation or crops (Thenkabail et al., 2000, 2002). Plant moisture sensitivity is best detected in the visible and NIR portion of the spectrum at 0.985 μm (Penuelas et al., 1995; Thenkabail et al., 2000). At this wavelength, direct measurements of water vapor in and over vegetation canopies are feasible (Richery et al., 1989). Seven of the nine wavebands in 0.400–1.050 μm found to be optimal in this research were also found optimal in Thenkabail et al. (2002).

Seven wavebands (in 0.400–1.050 μm) found to be optimal in this research were also found to be optimal in the 12 wavebands recommended by Thenkabail et al. (2002). The seven wavebands (Table 6) (with deviation from Thenkabail et al., 2002 within parentheses) were: $\lambda_1 = 0.495$ nm (-5 nm), $\lambda_2 = 0.555$ μm (-5 nm), $\lambda_3 = 0.655$ μm (-5 nm), $\lambda_4 = 0.675$ μm (-5 nm), $\lambda_5 = 0.705$ μm (-5 nm), $\lambda_8 = 0.915$ μm ($+5$ nm), and $\lambda_9 = 0.985$ μm ($+10$ nm). Even these differences were due to aggregating wavebands to 10-nm bands in this study, compared to much narrower (1.43-nm-wide) bands of earlier studies (see Table 2). This is a remarkable reaffirmation of the best wavebands to study agriculture and vegetation in the VNIR. The other two bands in the 0.400–1.050 μm range (Table 6), $\lambda_6 = 0.735$ μm and $\lambda_7 = 0.885$ μm ($+10$ nm), were somewhat different in Thenkabail et al. (2002) with red-edge (0.720 μm) and NIR (0.845 nm) wavebands. Such differences are to be expected mainly as a result of inclusion in this study: (a) SWIR portion of the spectrum; (b) vegetation (shrubs,

grasses, and weeds), in addition to agricultural crops; and (c) complexities of mixed cropping and vegetation systems. The earlier study by Thenkabail et al. (2002) was limited to crops and in the 0.400–1.050 μm portion of the spectrum. Substituting the additional wavebands of earlier study in 0.400–1.050 μm will be 13 new bands in 1.051–2.500 μm (Table 6). Little attention is paid to far near-infrared (FNIR; 1.051–1.300 μm) portion of the spectrum. Results (Table 6; Fig. 7) showed that five wavebands of particular importance are $\lambda_{10} = 1.085$ μm, $\lambda_{11} = 1.135$ μm, $\lambda_{12} = 1.215$ μm, $\lambda_{13} = 1.245$ μm, and $\lambda_{14} = 1.285$ μm. λ_{12} (1.215 μm) is the plant water absorption trough with $\lambda_{10} = 1.085$ μm and $\lambda_{14} = 1.285$ μm reflective peaks. The addition of two FNIR bands, for example, increased accuracies in classifying four weed species to 85.35% from 73.74% without them.

The ESWIR (1.300–1.900 μm) and FSWIR (1.900–2.500 μm) are very sensitive to changes (or differences) in moisture and biochemical properties such as in lignin (a polymer of phenylpropanoid), starch (main food storage molecule), and cellulose (D-glucose polymer) (see Elvidge, 1990). The most sensitive wavebands in ESWIR were 1.445 nm, 1.675 μm, and 1.725 μm (Table 6). In ESWIR, vegetation has a relatively low reflectance due to absorption primarily by leaf water. In the FSWIR, the best wavebands were centered at 2.005, 2.035, 2.235, 2.295, and 2.345 μm (Table 6). These wavebands are sensitive to a complex mix of healthy and senescing vegetation (Thenkabail et al., 1994a), and crop and leaf moisture variations (Ripple, 1986). Cellulose, which typically has one-third to one-half dry weight, and lignin, which makes up 10–35% of dry weight (Kumar et al., 2001), absorb heavily in 2.345, 2.295, and 2.345 μm (Elvidge, 1990).

3.5.1. Comparison with Hyperion wavebands

The Hyperion, the first spaceborne hyperspectral sensor, also gathers data in 0.400–2500 μm, but in 10-nm width.

t6.1 Table 6
t6.2 Optimal hyperspectral wavebands in 0.400–2.500 μm[a,b]

Waveband number	Waveband center (μm)	Frequency of occurrence	Waveband name	Importance for vegetation and agriculture[c]
Ultraviolet				
1	0.495	9	UV	Sensitive to senescing, carotenoid, browning, and soil background
Visible				
2	0.555	5	Green1	Green peak, sensitive to total chlorophyll
3	0.655	6	RED1	Absorption premaxima, sensitive to biomass and soil background
4	0.675	16	RED2	Absorption maxima, greatest soil–crop contrast in 350–2500 nm
Red edge				
5	0.705	6	Red edge1	Start of rapid change of slope, sensitive to vegetation stress and dynamics
6	0.735	9	Red edge2	End of rapid change of slope, sensitive to vegetation stress and dynamics
NIR				
7	0.885	5	NIR1	NIR prepeak; sensitive to total chlorophyll, biomass, LAI, and protein
8	0.915	6	NIR2	NIR peak, sensitive to total chlorophyll, biomass, LAI, and protein
MSNIR				
9	0.985	5	MSNIR	Moisture absorption trough in NIR, sensitive to plant moisture
FNIR				
10	1.085	9	FNIR1	Reflectance peak 1 in 1050–1300 nm, sensitive to biomass and LAI
11	1.135	5	FNIR2	Reflectance postpeak 1 in 1050–1300 nm, sensitive to biomass and LAI
12	1.215	10	FNIR3	Moisture absorption trough in FNIR, sensitive to plant moisture
13	1.245	14	FNIR4	Reflectance prepeak 2 in 1050–1300 nm, sensitive to biomass and LAI
14	1.285	8	FNIR4	Reflectance peak 2 in 1050–1300 nm, sensitive to biomass and LAI
Early mid-infrared (EMIR)				
15	1.445	7	EMIR1	Moisture absorption trough in EMIR, sensitive to plant moisture
16	1.675	6	EMIR3	Reflectance peak 1 in MIR; sensitive to lignin, biomass, and starch
17	1.725	5	EMIR4	Reflectance postpeak 2 in MIR; sensitive to biomass, cellulose, and lignin
Far mid-infrared (FMIR)				
18	2.005	17	FMIR1	Moisture absorption trough 1 in FMIR, sensitive to plant moisture
19	2.035	6	FMIR2	Moisture absorption trough 2 in FMIR, sensitive to plant moisture
20	2.235	6	FMIR3	Reflectance peak 2 in MIR; sensitive to lignin, biomass, and starch
21	2.295	9	FMIR4	Reflectance peak 2 in MIR; sensitive to soil background and stress
22	2.345	13	FMIR5	Absorption maxima 2 MIR; sensitive to crop stress, lignin, and starch

Waveband centers determined based on: (a) principal component analysis, (b) lambda–lambda R^2 models, and (c) stepwise discriminant analysis (Wilk's lambda).

[a] Waveband width is 10 nm for all bands.

[b] When two very close wavebands (e.g., 1.245 and 1.235 μm) provide a high frequency of occurrence, tests of redundancy such as correlation between bands or with biomass were performed to see whether the two bands provide essentially similar information. That being the case (as in the case of 1.245 and 1.235 μm), the waveband that was more frequently occurring of the two bands (e.g., 1.245 μm) was selected, leaving out the other (to avoid redundant information).

[c] Importance of wavebands is gathered from the works of Blackburn (1998), Carter (1997), Elvidge and Chen (1995), Kumar et al. (2001), Thenkabail (2002), and Thenkabail et al. (1999, 2000, 2002).

Thenkabail et al. (2004) established the best Hyperion 635 wavebands in a study of African rainforest vegetation. Since 636 this study was in African savannas, a direct comparison with 637 Hyperion study (Thenkabail et al., 2004) is not possible. 638 However, a cursory evaluation of band centers of the best 639 bands found in this study with the band centers of the best 640 Hyperion bands (Thenkabail et al., 2004) is useful to assess 641 the overall response to diverse vegetation from different 642 platforms. The results showed that the band centers of 13 of 643 the 22 wavebands of this study (outside the brackets) were 644 within ± 0.017 μm of the band centers of Hyperion best 645 bands (within parentheses) (Note: when no waveband in- 646 formation exists within parentheses, it indicates the absence 647 of comparable wavebands.): $\lambda_1 = 0.495$ μm (+ 0.004 μm), 648 $\lambda_2 = 0.555$ μm, $\lambda_3 = 0.655$ μm, $\lambda_4 = 0.685$ μm (− 0.003 μm), 649 $\lambda_5 = 0.705$ μm, $\lambda_6 = 0.735$ μm (− 0.013 μm), $\lambda_7 = 0.885$ μm 650

651 (+ 0.010 μm), $\lambda_8 = 0.925$ μm, $\lambda_9 = 0.985$ μm, $\lambda_{10} = 1.085$ μm
652 (+ 0.009 μm), $\lambda_{11} = 1.135$ μm ((+ 0.010 μm), $\lambda_{12} = 1.215$ μm
653 (0 μm), $\lambda_{13} = 1.245$ μm, $\lambda_{14} = 1.280$ μm (+ 0.006 μm),
654 $\lambda_{15} = 1.450$ μm (+ 0.017 μm), $\lambda_{16} = 1.690$ μm, $\lambda_{17} = 1.725$
655 μm (− 0.015 μm), $\lambda_{18} = 2.000$ μm, $\lambda_{19} = 2.035$ μm (− 0.013
656 μm), $\lambda_{20} = 2.235$ μm, $\lambda_{21} = 2.285$ μm (− 0.016), and
657 $\lambda_{22} = 2.330$ μm (− 0.015 μm) (see Table 6). The results
658 indicate that a significant number of wavebands have similar
659 or near-similar waveband centers across vegetation types. It
660 is, however, necessary to avoid keeping the wavebands too
661 narrow. It appears that a band width of about 0.030 μm is
662 likely to cover a diverse range of vegetation.

663

664 *3.5.2. Accuracy assessments of hyperspectral wavebands*
665 *for determining optimal bands*
666   The wavebands were organized and their frequency of
667 occurrence (Fig. 7) determined their ranking (Table 6). The
668 ranking of the best wavebands were used to input bands
669 for accuracy assessment and for classifying species. This
670 has been illustrated for classifying the five weed species
671 (Table 7a). Similar patterns follow for grass, shrub, or crop
672 species, and hence we report only for weed species.
673 Addition of NIR and moisture-sensitive NIR (MSNIR)

674 increased the accuracies by another 7% to a total overall
675 accuracy of 74%.
676   Overall accuracies and Khat were calculated for the best
677 1 band, best 2 bands, and so on, to all 168 bands (e.g., Fig.
678 8a and b). The best bands were decided based on their
679 frequency of occurrence (Table 6). For the first 10–15
680 wavebands, overall accuracies (and Khat) increased rapidly
681 with every addition of waveband. For classifying the five
682 weed species, the overall accuracies increased from 56% for
683 the 3 bands, to 72% for 7 bands, to 90% for 13 bands, to
684 98% for 22 bands (Fig. 8a). Similarly, trends were obtained
685 for crop species (Fig. 8b), shrub species, and grass species.
686 For crops with 13 bands, the accuracies were 90%, but
687 required over 50 bands to reach 98%, highlighting the
688 practical limits of hyperspectral data beyond a certain point,
689 as pointed out by Okin et al. (2001).
690   The highest increase of 15% was when FNIR bands
691 1.085, 1.135, 1.215, 1.245, and 1.285 μm were added,
692 followed by 8% for SWIR. The role of FNIR bands is
693 surprisingly neglected in most sensor designs. The results
694 in this research indicate some of the most valuable wave-
695 bands to study vegetation, and crops are present in this
696 wavelength portion. The starch absorption at 1.445 is
697 prominent (Danson et al., 1992) and the other ESWIR
698 wavebands have significant relationships between leaf
699 water density and leaf reflectance (Danson et al., 1992).
700 The FSWIR wavebands are highly correlated with leaf
701 cover and relative water content (Ripple, 1986). Jakubaus-
702 kas and Price (1997) found that the biotic factors relating
703 to the gross physical structure of the canopy (height,
704 biomass, and LAI) are best predicted using the TM
705 middle-infrared bands (TM5 and TM7) or a combination
706 of visible (TM1, TM2, or TM3) and middle-infrared bands.
707 Availability of narrow-focused wavebands in the region
708 can further strengthen the quantitative characterization of
709 vegetation (Boyd et al., 1996; Ripple, 1986). An important
710 point to note is that both FNIR and SWIR bands provide
711 an additional "missing" (or unique) information not avail-
712 able VNIR. Within SWIR, ESWIR is a far more important
713 than FSWIR.
714   The error matrix (Table 7b) showing the classification of
715 five weed species is determined using the discriminant
716 model and is illustrated for the 22 best hyperspectral bands.
717 The errors of omission and commission were low (0–12%).
718 The maximum error occurred between species (omission)
719 *Cassia obtusifolia* and *A. conyzoides* with 18.6% (Table
720 7b). The overall accuracy of 97% (Khat = 96%) indicated
721 that the best 22 bands provide near-maximal solution
722 (Table 7b).

723

724 *3.5.3. Accuracy assessment of agricultural crops: compar-*
725 *ison with independent datasets*
726   The hyperspectral accuracy assessments of agricultural
727 crops of this study in African savannas (Fig. 8b) were
728 compared with accuracy assessments of two other inde-
729 pendent datasets obtained in the representative desert

t7.1   Table 7a
t7.2   Overall accuracies and Khat

Rationale	Waveband centers (μm)	Weeds		
		Overall accuracy (%)	Increase in overall accuracy (%)	Khat (%)
(1) *Four bands*: UV, Visible	0.495, 0.555, 0.655, 0.675	54		43
(2) *Six bands*: UV, Visible, and red edge	0.495, 0.555, 0.655, 0.675, 0.705, 0.735	67	13	56
(3) *Nine bands*: UV, Visible, red edge, NIR, and MSNIR	0.495, 0.555, 0.655, 0.675, 0.705, 0.735, 0.885, 0.915, 0.985	74	7	66
(4) *Fourteen bands*: UV, Visible, red edge, NIR, MSNIR, and FNIR	0.495, 0.555, 0.655, 0.675, 0.705, 0.735, 0.885, 0.915, 0.985, 1.085, 1.135, 1.215, 1.245, 1.285	89	15	81
(5) *Seventeen bands*: UV, Visible, red edge, NIR, MSNIR, FNIR, and EMIR	0.495, 0.555, 0.655, 0.675, 0.705, 0.735, 0.885, 0.915, 0.985, 1.085, 1.135, 1.215, 1.245, 1.285, 1.445, 1.675, 1.725	95	6	94
(6) *Twenty-two bands*: UV, Visible, red edge, NIR, MSNIR, FNIR, and FMIR	0.495, 0.555, 0.655, 0.675, 0.705, 0.735, 0.885, 0.915, 0.985, 1.085, 1.135, 1.215, 1.245, 1.285, 1.445, 1.675, 1.725, 2.005, 2.035, 2.235, 2.295, 2.345	97	2	96

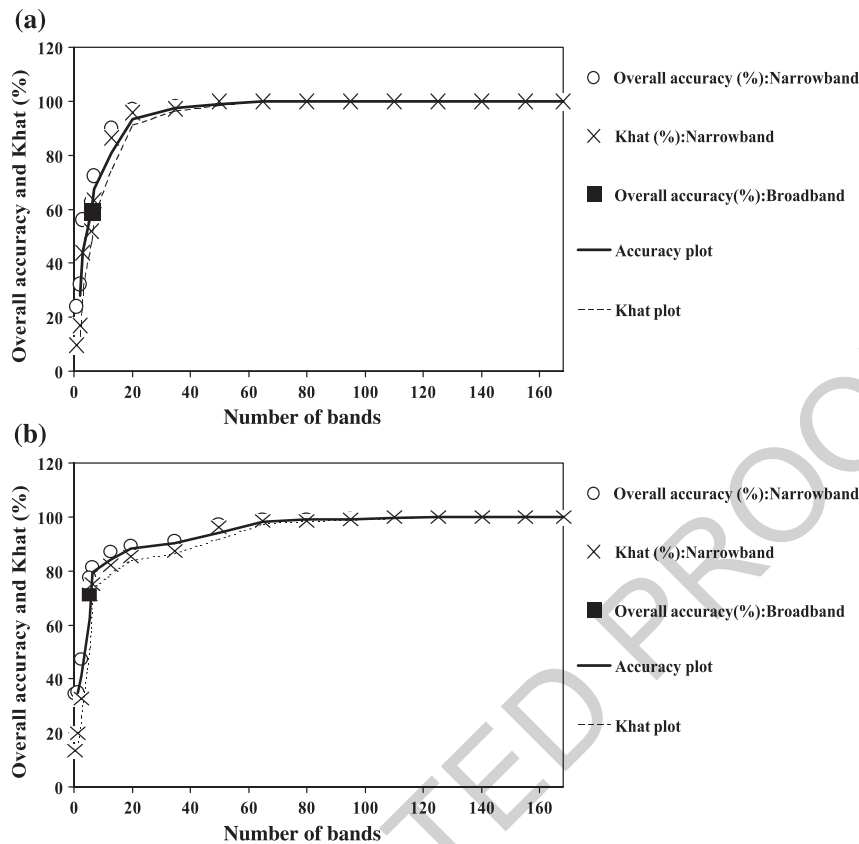t7.11   Accuracies in classifying and separating five weed species.

Fig. 8. (a) Accuracy assessment. Overall accuracies and Khat when classifying five weed species (*A. conyzoides*, *A. africana*, *C. obtusifolia*, *C. odorata,* and *T. bracteolata*) from the four ecoregions of the African savannas. (b) Accuracy assessment. Overall accuracies and Khat when classifying six crop species (cassava—*Manihot esculenta,* corn—*Zea mays,* cowpea—*Vigna unguiculata,* groundnut—*Arachis hypogaea*, rice—*Oryza sativ,* and soybean—*Glycine max*) from the four ecoregions of the African savannas.

margin benchmark area of the world based in Syria. The 730
accuracy assessments are presented for the independent 731
datasets of the wet season crops of 1998 (Fig. 9a) and for 732

dry season crops of 1997 (Fig. 9b). Much like the accuracy 733
assessments of the present datasets for agricultural crops 734
(Fig. 8b), the independent datasets provided remarkably 735
similar results, reaching overall accuracies (and Khat) of 736
over 90% for 30 bands (Fig. 9a and b). In each case, the 737
most rapid rise in accuracies was in the first 10–15 bands. 738
The results further reaffirm that to obtain the best crop and 739
vegetation information, 30 or less wavebands are needed. 740
It is also obvious from Fig. 9a that the broadband data (of 741
TM) had substantially lower accuracies when compared 742
with narrowband data, further confirming the results found 743
in Section 3.3. 744

3.5.4. Accuracy assessment of vegetation and crop species: broad and narrowbands
746
747

Discriminant model (see Section 3.3) was used to clas- 748
sify and place each observation of shrub, grass, weed, and 749
crop species into a class in which it has the smallest 750
generalized squared distance. Based on the correctly classi- 751
fied samples, overall accuracy assessments were performed 752
for each species using narrowbands and broadbands (Table 753
8). In most cases, even the six best VNIR narrowbands 754
(without any SWIR bands) performed slightly better than 755
the six simulated ETM$^+$ broadbands (with SWIR bands). 756

t8.1	Table 7b						
t8.2	Errors and accuracies[a]						
t8.3	Observed weed species[b]	Classified weed species[b]					
		ag	as	cao	cho	te	Commission errors (%)
t8.4							
t8.5	ag	56	0	3	1	0	6.67
t8.6		93.33	0.00	5.00	1.67	0.00	
t8.7	as	0	29	0	0	0	0
t8.8		0.00	100.00	0.00	0.00	0.00	
t8.9	cao	0	0	22	0	0	0
t8.10		0.00	0.00	100.00	0.00	0.00	
t8.11	cho	0	0	0	67	0	0
t8.12		0.00	0.00	0.00	100.00	0.00	
t8.13	te	0	0	0	1	19	5
t8.14		0.00	0.00	0.00	5.00	95.00	
t8.15	Omission errors (%)	0	0	12	6.9	0	

Classification accuracy matrix using discriminant model for weeds species
t8.16 when all 22 best bands (Table 4 and last row in Table 5) are used.

t8.17 [a] Overall accuracy = 97% (193/198); Khat = 96% (see Thenkabail, 2002 for calculations).

t8.18 [b] For the abbreviation of weed species, see Fig. 3d.
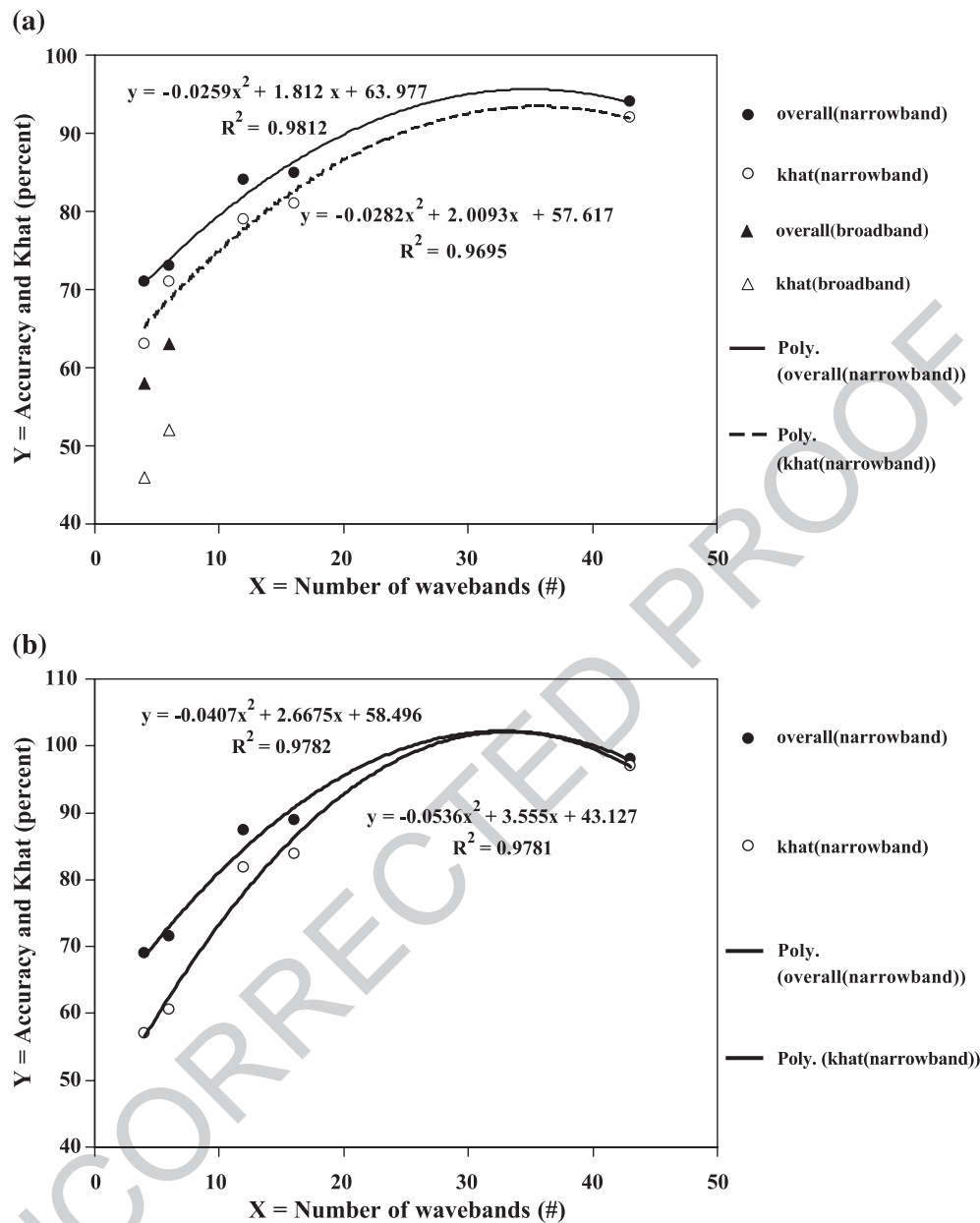
(a)

(b)

Fig. 9. (a) Accuracy assessment of the 1997 dry season crop data. Overall accuracy and Khat in classifying five dry season crops (cotton, corn, soybean, potato, and sunflower) in a representative semiarid benchmark area for the world based in Syria. (b) Accuracy assessment of the 1998 wet season crop data. Overall accuracy and Khat in classifying six wet season crops (wheat, barley, chickpea, lentil, vetch, and cumin) in a representative semiarid benchmark area for the world based in Syria.

For each species, accuracies in identifying species increased rapidly, reaching a plateau at about 94% when 13–22 more wavebands were used (Table 8).

4. Conclusions

The study resulted in recommending 22 best narrow-bands (from 168 hyperspectral bands), in the 0.350–2.500 μm range, to discriminate natural vegetation species of shrubs, grasses, weeds, and agricultural crops based on data from African savannas. The most frequently occurring waveband centers or ranges in spectro-biophysical models were (when bandwidths are not mentioned, they are 10 nm wide): $\lambda_1 = 0.495$ μm, $\lambda_2 = 0.555$ μm, $\lambda_3 = 0.645 - 0.665$ μm, $\lambda_4 = 0.675 - 0.695$ μm, $\lambda_5 = 0.705$ μm, $\lambda_6 = 0.735$ μm, $\lambda_7 = 0.885$ μm, $\lambda_8 = 0.915 - 0.935$ μm, $\lambda_9 = 0.985$ μm, $\lambda_{10} = 1.085$ μm, $\lambda_{11} = 1.135$ μm, $\lambda_{12} = 1.215$ μm, $\lambda_{13} = 1.235 - 1.255$ μm, $\lambda_{14} = 1.275 - 1.285$ μm, $\lambda_{15} = 1.445 - 1.455$ μm, $\lambda_{16} = 1.675 - 1.705$ μm, $\lambda_{17} = 1.715 - 1.735$ μm, $\lambda_{18} = 1.985 - 2.015$ μm, $\lambda_{19} = 2.025 - 2.045$ μm, $\lambda_{20} = 2.235$ μm, $\lambda_{21} = 2.275 - 2.295$

t9.1 Table 8

t9.2 Narrowband vs. broadband overall classification accuracies for vegetation and crop species

Category	Waveband center (nm)				
	Sample size	Narrowband accuracies[a] (%)		Broadband (simulated ETM$^+$)[b] accuracies (%) (six bands)	Difference in accuracy (%) between optimal narrowbands and ETM$^+$ broadbands
		Visible–red edge–NIR–MSNIR	Optimal bands		
		Six best narrowbands in VNIR (μm): 0.490, 0.550, 0.675, 0.720, 0.845, 0.975 (six bands)	Best bands from Table 3 (12–21 optimal bands)		
Agricultural crops					
Corn (*Zea mays*)	146	75	90	68	23
Cassava (*Manihot esculenta*)	22	100	100	82	18
Cowpea (*Vigna unguiculata*)	18	100	100	61	39
Groundnut (*Arachis hypogaea*)	34	74	88	79	9
Rice (*Oryza sativa*)	35	86	100	80	20
Soybean (*Glycine max*)	37	81	97	54	43
Shrub species					
Isoberlina tomentosa	39	74	95	74	21
Piliostigma thoniningii	38	84	90	81	9
Pteleopsis habeensis	20	100	100	85	15
Grass species					
Brachiaria jubata	32	53	94	81	13
Brachiaria stigmatisata	72	78	92	69	22
Digitaria sp.	30	63	80	40	40
Imperata cylindrica	45	71	91	64	27
Weed species					
Ageratum conyzoides	60	65	93	57	37
Aspilia africana	29	59	100	83	17
Cassia obtusifolia	22	86	100	77	23
Chromolaena odorata	67	64	97	83	15
Tephrosia bracteolata	20	90	95	85	10

t9.32 Classification accuracies determined by discriminant model for: (a) hyperspectral narrowbands and (b) simulated ETM$^+$ broadbands.

[a] Narrowband accuracies were computed using wavebands from Table 4. An increase in accuracy of classification with an increase in number of wavebands reaches a plateau (optimal) at some stage. Optimal accuracies were taken when the addition of waveband did not lead to statistically significant increases in accuracies. Typically, this happened anywhere between 12 and 22 bands.

[b] Broadband accuracies were computed for the six nonthermal ETM$^+$ wavebands. The ETM$^+$ bands were: ETM$^+$ 1 = 0.450–0.515 μm; ETM$^+$ 2 = 0.525–0.605 μml ETM$^+$ 3 = 0.630–0.690 μm; ETM$^+$ 4 = 0.750–0.900 μm; ETM$^+$ 5 = 1.550–1.750 μm; and ETM$^+$ 6 = 2.090–2.350 μm.

776 μm, and λ_{22} = 2.315–2.345 μm (see Table 6). The wave-
777 bands were clustered in such a way that the narrow wave-
778 bands in ESWIR (1.300–1.900 nm) were the most
779 prominent by explaining 65% of all variabilities in data.
780 This was followed by red bands (0.600–0.700 μm), which
781 explained 19% variability, and FSWIR (1.900–2.500 μm),
782 which explained 11% variability. Of the 22 recommended
783 wavebands, eight were in ESWIR ($\lambda_{15}–\lambda_{22}$) and four in
784 FNIR ($\lambda_{11}–\lambda_{14}$).

785 The results, when compared with other hyperspectral
786 studies (Thenkabail et al., 2000, 2002, 2004), indicate that
787 a significant number of wavebands have similar or near-
788 similar waveband centers across vegetation types. However,
789 it is necessary to avoid keeping the wavebands too narrow.
790 A band width of about 0.030 μm is likely to cover a diverse
791 range of vegetation in rainforests, savannas, or desert
792 margin agriculture.

793 A 97% reduction in data volume is feasible when
794 hundreds of hyperspectral wavebands are reduced to the
795 first five principal components, which still explain about
796 95% variability in data. The ESWIR bands dominated the
797 PC1 with a 62% frequency of occurrence, followed by the
798 red bands in PC2 explaining 20% variability. The FSWIR
799 bands dominated PC3–PC5 in all, explaining an additional
800 12% of the variability.

801 Overall accuracies of about 90% were attained when
802 13–22 best narrowbands are used in classifying vegeta-
803 tion and agricultural crop species. Beyond 22 bands,
804 accuracies only increase marginally, explaining 4–8%
805 additional variability up to 30 bands. Future generations
806 of satellites are either likely to carry specialized optimal
807 sensors, with wavebands as recommended in Table 6,
808 focusing to gather data for targeted applications or gath-
809 ering data from hundreds of hyperspectral narrowbands
810 like Hyperion from which users will have to extract
811 appropriate optimal wavebands relevant for their applica-
812 tion. In both cases, the findings of this research will be of
813 value.

Acknowledgements

References

Aoki, M., Yabuki, K., & Totsuka, T. (1981). An evaluation of chlorophyll content of leaves based on the spectral reflectivity in several plants. *Research Report of the National Institute for Environmental Studies of Japan, 66*, 125–130.

Bauer, M. E., Daughtry, C. S. T., & Vanderbilt, V. C. (1981). *Spectral–agronimic relationships of corn, soybean, and wheat canopies* (17 pp.). Report SR-P1-04187. West Lafayette, IN: Laboratory for Applications of Remote Sensing, Purdue University.

Bishop, Y., Fienberg, S., & Holland, P. (1975). *Discrete multivariate analysis—theory and practice*. Cambridge, MA: MIT Press.

Blackburn, G. A. (1998). Spectral indices for estimating photosynthetic pigment concentrations: A test using senescent tree leaves. *International Journal of Remote Sensing, 19*(4), 657–675.

Blackburn, G. A. (1999). Towards the remote sensing of matorral vegetation physiology: Relationships between spectral reflectance, pigment, and biophysical characteristics of semiarid bushland canopies. *Remote Sensing of Environment, 70*, 278–292.

Blackburn, G. A., & Steele, C. M. (1999). Towards the remote sensing of matorral vegetation physiology: Relationships between spectral reflectance, pigment, and biophysical characteristics of semiarid bushland canopies. *Remote Sensing of Environment, 70*, 278–292.

Bork, E. W., West, N. E., & Price, K. P. (1999). Calibration of broad- and narrow-band spectral variables for rangeland cover component quantification. *International Journal of Remote Sensing, 20*(18), 3641–3662.

Boyd, D. S., Foody, G. M., Curran, P. J., Lucas, R. M., & Honzak, M. (1996). An assessment of radiance in Landsat TM middle and thermal infrared wavebands for the detection of tropical forest regeneration. *International Journal of Remote Sensing, 17*, 249–261.

Broge, N. H., & Leblanc, E. (2000). Comparing prediction power and stability of broadband and hyperspectral vegetation indices for estimation of green leaf area index and canopy chlorophyll density. *Remote Sensing of Environment, 76*, 156–172.

Carter, G. A. (1994). Ratios of leaf reflectances in narrow wavebands as indicators of plant stress. *International Journal of Remote Sensing, 15*, 697–703.

Carter, G. A. (1998). Reflectance bands and indices for remote estimation of photosynthesis and stomatal conductance in pine canopies. *Remote Sensing of Environment, 63*, 61–72.

Clevers, J. G. P. W. (1999). The use of imaging spectrometry for agricultural applications. *ISPRS Journal of Photogrammetry and Remote Sensing, 54*, 299–304.

Congalton, R. G. (1988). A comparison of sampling schemes used in generating error matrices for assessing the accuracy of maps generated from remotely sensed data. *Photogrammetric Engineering and Remote Sensing, 54*(5), 593–600.

Congalton, R. G. (1991). A review of assessing the accuracy of classifications of remotely sensed data. *Remote Sensing of Environment, 37*, 35–46.

Congalton, R. G., & Mead, R. A. (1983). A quantitative method to test for consistency and correctness in photointerpretation. *Photogrammetric Engineering and Remote Sensing, 49*(1), 69–74.

Curran, P. J. (1994). Imaging spectrometry. *Progress in Physical Geography, 18*(2), 247–266.

Curran, P. J., Dungan, J. L., Macler, B. A., & Plummer, S. E. (1991). The effect of a red leaf pigment on the relationship between red-edge and chlorophyll concentration. *Remote Sensing of Environment, 35*, 69–75.

Danson, F. M., Steven, M. D., Malthus, T. J., & Clark, J. A. (1992). High-spectral resolution data for determining leaf water content. *International Journal of Remote Sensing, 13*, 461–470.

Elvidge, C. D. (1990). Visible and near infrared reflectance characteristics of dry plant materials. *International Journal of Remote Sensing, 11* (1775–1795).

Elvidge, C. D., & Chen, Z. (1995). Comparison of broadband and narrow-band red and near-infrared vegetation indices. *Remote Sensing of Environment, 54*, 38–48.

Elvidge, C. D., Chen, Z., & Groeneveld, D. P. (1993). Detection of trace quantities of green vegetation in 1990 AVIRIS data. *Remote Sensing of Environment, 44*, 271–279.

Food and Agricultural Organization of United Nations (FAO). 1978. *Report on the agro-ecological zones project: Vol. I. Methodology and results for Africa* (p. 158). World Soil Resources Report 48/1, Rome.

Gao, J. (1999). A comparative study on spatial and spectral resolutions of satellite data in mapping mangrove forests. *International Journal of Remote Sensing, 20*(14), 2823–2833.

Jakubauskas, M. E., & Price, K. P. (1997). Empirical relationships between biotic and spectral factors of Yellowstone lodgepole pine forests. *Photogrammetric Engineering and Remote Sensing, 63*(11).

Janetos, A. C., & Justice, C. O. (2000). Land cover and global productivity: A measurement strategy for the NASA programme. *International Journal of Remote Sensing, 21*(6 &), 1491–1512.

Kumar, L., Schmidt, K. S., Dury, S., & Skidmore, A. K. (2001). Review of hyperspectral remote sensing and vegetation science. In F. Van Der Meer (Ed.), *Hyperspectral remote sensing*. Dordrecht: Kluwer Academic Press.

Lichtenthaler, H. K., Gitelson, A. A., & Lang, M. (1996). Non-destructive determination of chlorophyll content of leaves of a green and an aurea mutant of tobacco by reflectance measurements. *Journal of Plant Physiology, 148*, 483–493.

Lyon, J. G., Yuan, D., Lunetta, R. S., & Elvidge, C. D. (1998). A change detection experiment using vegetation indices. *Photogrammetric Engineering and Remote Sensing, 64*, 143–150.

Mariotti, M., Ercoli, L., & Masoni, A. (1996). Spectral properties of iron-deficient corn and sunflower leaves. *Remote Sensing of Environment, 58*, 282–288.

Mass, S. J. (2000). Linear mixture modeling approach for estimating cotton canopy ground cover using satellite multispectral imagery. *Remote Sensing of Environment, 72*(3), 304–308.

McGwire, K., Minor, T., & Fenstermaker, L. (2000). *Hyperspectral mixture modeling for quantifying sparse vegetation cover in arid environments. 72*(3), 360–374.

Okin, G. S., Roberts, D. A., Murray, B., & Okin, W. J. (2001). Practical limits on hyperspectral vegetation discrimination in arid and semiarid environments. *Remote Sensing of Environment, 77*, 212–225.

Penuelas, J., Filella, I., Biel, C., Serrano, L., & Save, R. (1993). The

939 reflectance at the 950–970 region as an indicator of plant water status. *International Journal of Remote Sensing*, *14*(10), 1887–1905.

941 Penuelas, J., Filella, I., Lloret, P., Munoz, F., & Vilajeliu, M. (1995). Reflectance assessment of mite effects on apple trees. *International Journal of Remote Sensing*, *16*, 2727–2733.

944 Rao, C. R. (1973). *Linear statistical inference and its applications*. New York: Wiley.

946 Richery, J. E., Adams, J. B., & Victoria, R. L. (1989). Synoptic-scale hydrological and biogeochemical cycles in the amazon river basin: A modelling and remote sensing perspective. In R. J. Hobbs, & H. A. Mooney (Eds.), *Remote sensing of biosphere functioning. Ecological Studies, vol. 79* (pp. 249–268). New York: Springer-Verlag.

951 Ripple, W. J. (1986). Spectral reflectance relationships to leaf water stress. *Photogrammetric Engineering and Remote Sensing*, *52*(10), 1669–1675.

954 SAS Institute (2000). *SAS/STAT user's guide and software release, 6.12 edition*. Cary, NC: SAS Institute.

956 Schepers, J. S., Blackmer, T. M., Wilhelm, W. W., & Resende, M. (1996). Transmittance and reflectance measurements of corn leaves from plants with different nitrogen and water supply. *Journal of Plant Physiology*, *148*, 523–529.

960 Shaw, D. T., Malthus, T. J., & Kupiec, J. A. (1998). High-spectral resolution data for monitoring Scots pine (*Pinus sylvestris* L.) regeneration. *International Journal of Remote Sensing*, *19*(13), 2601–2608.

963 Thenkabail, P. S. (2002). Optimal hyperspectral narrowbands for discriminating agricultural crops. *Remote Sensing Reviews*, *20*(4), 257–291.

966 Thenkabail, P. S. (2003). Biophysical and yield information for precision farming from near-real-time and historical Landsat TM images. *International Journal of Remote Sensing*, *24*(14), 839–877.

969 Thenkabail, P. S. (2004). Inter-sensor relationships between IKONOS and Landsat-7 ETM+ NDVI data in three ecoregions of Africa. *International Journal of Remote Sensing*, *25*(2), 389–408.

972 Thenkabail, P. S., Enclona, E. A., Ashton, M. S., Legg, C., & Jean De Dieu, M. (2004). Hyperion, IKONOS, ALI, and ETM+ sensors in the study of African rainforests. *Remote Sensing of Environment*, *90*, 23–43.

975 Thenkabail, P. S., Hall, J., Lin, T., Ashton, M. S., Harris, D., & Enclona, E. A. (2003). Detecting floristic structure and pattern across topographic and moisture gradients in a mixed species Central African forest using IKONOS and Landsat-7 ETM+ images. *International Journal of Applied Earth Observation and Geoinformation*, *4*, 255–270.

980 Thenkabail, P. S., & Nolte, C. (2003, May). Regional characterization of inland valley agroecosystems in West and Central Africa using high-resolution remotely sensed data (Chapter 8). *GIS for water resources and watershed management by John G. Lyon* (p. 278). Ann Arbor Press, ASIN 1575040905.

985 Thenkabail, P. S., Smith, R. B., & De-Pauw, E. (2000). Hyperspectral vegetation indices for determining agricultural crop characteristics. *Remote Sensing of Environment*, *71*, 158–182.

988 Thenkabail, P. S., Smith, R. B., & De-Pauw, E. (2002). Evaluation of narrowband and broadband vegetation indices for determining optimal hyperspectral wavebands for agricultural crop characterization. *Photogrammetric Engineering and Remote Sensing*, *68*(6), 607–621.

992 Thenkabail, P. S., Ward, A. D., & Lyon, J. G. (1994a). Landsat-5 Thematic Mapper models of soybean and corn crop characteristics. *International Journal of Remote Sensing*, *15*, 49–61.

995 Thenkabail, P. S., Ward, A. D., Lyon, J. G., & Merry, C. J. (1994b). Thematic Mapper vegetation indices for determining soybean and corn crop growth parameters. *Photogrammetric Engineering and Remote Sensing*, *60*(4), 437–442.

999 Tucker, C. J. (1977). Spectral estimation of grass canopy variables. *Remote Sensing of Environment*, *6*, 11–26.

1001